NASA TECHNICAL MEMORANDUM

NASA TM X-58056

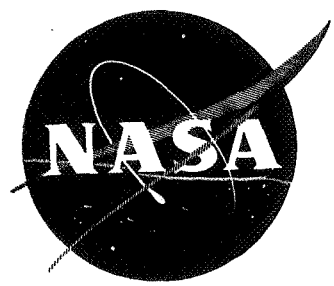

THE PROBLEM OF AN ELASTIC LAYER WITH A CYLINDRICAL HOLE SUBJECTED TO A NONUNIFORM AXISYMMETRIC RADIAL DISPLACEMENT

A Thesis Presented to the
Faculty of the Department of Mechanical Engineering
of the University of Houston
In Partial Fulfillment of
the Requirements for the Degree
Master of Science

NATIONAL AERONAUTICS AND SPACE ADMINISTRATION
MANNED SPACECRAFT CENTER
HOUSTON, TEXAS

NASA TM X-58056

THE PROBLEM OF AN ELASTIC LAYER WITH A CYLINDRICAL HOLE SUBJECTED TO A NONUNIFORM AXISYMMETRIC RADIAL DISPLACEMENT

David Stuart Grissom
Manned Spacecraft Center
Houston, Texas

ACKNOWLEDGEMENTS

I would like to acknowledge the following people for their contributions in the preparation of this thesis:

My advisor, Dr. C.D. Michalopoulos, Associate Professor of Mechanical Engineering, for suggesting this interesting problem to me and assisting me through to a successful completion.

Drs. Bart Childs, Ray Nachlinger and J.M. Nash for providing constructive criticism.

My co-workers, William C. Schneider and Clarence J. Wesselski, who, with their group discussions, helped me to overcome some of the daily problems I encountered. Special thanks to Mr. Schneider whose enthusiasm and understanding of problems in elasticity provided me with many insights into this field.

Mr. Fred Nau, who provided assistance in the numerical computations.

Mr. Robert T. Gunderson for suggesting changes to the written material to improve its technical clarity.

I also wish to extend my appreciation to Messrs. Nick Jevas and R.F. Smith, my immediate supervisors, for their willing and encouraging attitude toward my graduate studies.

Last, but above all, I am forever grateful to my

family. My wife, Linda, deserves much credit for the patience and understanding she has shown over the years. My children, David and Jill, must be credited for accepting something they were too young to understand.

ABSTRACT

A problem in the linear theory of elasticity is considered wherein a layer with a circular cylindrical hole is subjected to a nonuniform radial displacement. The deformation is imposed on the cylindrical boundary such that axisymmetric displacements and stresses result. The solution utilizes Navier's equations of elasticity. These equations are solved by use of extended Hankel transforms to obtain displacements. Shear and longitudinal stresses are obtained by transformed stress-strain relationships. Radial and circumferential stresses, however, are obtained directly by use of stress-strain equations.

The solution of a problem where the imposed radial displacement is a linear function of the axial coordinate is presented. Numerical results are given in graphical form for two different ratios of hole radius to layer thickness. The infinite integrals of the inversion formulas were evaluated numerically using Longman's technique for computing infinite integrals of oscillatory functions.

TABLE OF CONTENTS

LIST OF FIGURES

LIST OF SYMBOLS

a	radius of circular cylindrical hole
b	minimum imposed radial displacement
B	arbitrary constant
C	arbitrary constant
D	derivative operator with respect to z
E	Young's modulus
$f(\ )$	arbitrary function of ( )
h	layer thickness
I	integral approximated by series
i	index
J_τ	Bessel function, first kind, order τ
n	index
ρ_0	dummy variable in $R_0(\rho_0,\gamma)$ to compute roots
ρ_1	dummy variable in $R_1(\rho_1,\gamma)$ to compute roots
$P(\tau,\nu)$	series in asymtotic approximation for $J_\tau \& Y_\tau$
$Q(\tau,\nu)$	series in asymtotic approximation for $J_\tau \& Y_\tau$
r	radial coordinate
$R_0(s,r,a)$	$J_0(sr)\,Y_1(sa) - J_1(sa)\,Y_0(sr)$
$R_1(s,r,a)$	$J_1(sr)\,Y_1(sa) - J_1(sa)\,Y_1(sr)$
$\mathcal{R}_0$	forward transformation, zero-order
$\mathcal{R}_1$	forward transformation, first-order
$\mathcal{R}_0^{-1}$	inverse transformation, zero-order
$\mathcal{R}_1^{-1}$	inverse transformation, first-order

s	transform variable
u	radial displacement
$\overline{u}$	transformed radial displacement
V_i	ith term of series approximating integral
w	longitudinal displacement
$\overline{w}$	transformed longitudinal displacement
x	dummy variable
Y_τ	Bessel function, second kind, order τ
z	longitudinal coordinate
α	dimensionless variable a/h
β	dimensionless variable b/h
γ	dummy variable
δ	dummy variable
Δ	difference operator
ζ	dimensionless variable z/h
η	transform variable in nondimensional equations
θ	cylindrical coordinate
K_0	kernel of $\mathcal{R}_0^{-1}$
K_1	kernel of $\mathcal{R}_1^{-1}$
λ	Lame constant
μ	Lame constant
ν	Poisson's ratio
ρ	dimensionless variable r/h
σ_i	stress in i direction
$\overline{\sigma_i}$	transformed stress in i direction

ν	order of Bessel function
ϕ	angle of cylindrical boundary deformation
ξ	dummy variable
ω	dummy variable

CHAPTER I

INTRODUCTION

In 1964, Scott and Miklowitz[1] [1] introduced the use of extended Hankel transforms in a problem of elastic wave propogation. The problem was an infinite plate with a circular cylindrical hole. The cylindrical boundary was subjected to a uniform step radial displacement and the resulting axially-symmetric compressional waves were studied. No attempt was made to determine the state of stress in the body. Seco[2] introduced the use of this type of transformation in solving an axisymmetric heat conduction problem in 1969.

The extended Hankel transformations employed in this thesis are based on an expansion formula discovered by Weber[3] in 1873. Orr[4] rediscovered Weber's formula in 1909 by a method of contour integration. The formal proof of the Weber-Orr expansion formula was established in 1922 by Titchmarsh[5] who, in his book[6], broadened its use. The following expansion formulas are given by Titchmarsh[6] :

$$f(\tau) = \int_0^\infty \frac{s\, R_0(s,\tau;a)\, ds}{J_1^2(as) + Y_1^2(as)} \cdot \int_a^\infty \tau f(\tau)\, R_0(s,\tau;a)\, d\tau \qquad (1.1)$$

$$f(\tau) = \int_0^\infty \frac{s\, R_1(s,\tau;a)\, ds}{J_1^2(sa) + Y_1^2(sa)} \cdot \int_a^\infty \tau f(\tau)\, R_1(s,\tau;a)\, d\tau, \qquad (1.2)$$

---

[1] Numbers in brackets refer to the Bibliography at the end of the thesis.

where

$$R_0(s,\tau;a) = J_0(s\tau)\,Y_1(sa) - J_1(sa)\,Y_0(s\tau)$$

$$R_1(s,\tau;a) = J_1(s\tau)\,Y_1(sa) - J_1(sa)\,Y_1(s\tau)\,.$$

The same set of transforms used by Scott and Miklowitz [1] are employed in this thesis. Defining the zero and first-order transforms as

$$\mathcal{R}_0[f(\tau)] = \bar{f}_0(s) = \int_a^\infty \tau\, f(\tau)\, R_0(s,\tau;a)\, d\tau \qquad (1.3)$$

$$\mathcal{R}_1[f(\tau)] = \bar{f}_1(s) = \int_a^\infty \tau\, f(\tau)\, R_1(s,\tau;a)\, d\tau\,, \qquad (1.4)$$

respectively, it follows from Eqs. (1.1) and (1.2) that the inverse transforms are

$$\mathcal{R}_0^{-1}[\bar{f}_0(s)] = f(\tau) = \int_0^\infty \frac{s\,\bar{f}_0(s)\,R_0(s,\tau;a)\,ds}{J_1^2(sa) + Y_1^2(sa)} \qquad (1.5)$$

$$\mathcal{R}_1^{-1}[\bar{f}_1(s)] = f(\tau) = \int_0^\infty \frac{s\,\bar{f}_1(s)\,R_1(s,\tau;a)\,ds}{J_1^2(sa) + Y_1^2(sa)}\,. \qquad (1.6)$$

Properties of the transforms which are applicable to this thesis are presented in Appendix A.

The problem to be studied in this thesis is an outgrowth of the work done by Scott and Miklowitz. The aim of this study is to present a method for determining the static displacements and stresses throughout the elastic body posed

by Scott and Miklowitz for the case of a nonuniform radial displacement.

The statement of the problem and its analytical solution is presented in Chapter II. The technique used to evaluate the inverse transforms numerically is presented in Chapter III. Numerical results are given in Chapter IV and are followed by the Summary and Conclusions in Chapter V.

CHAPTER II

THE PROBLEM

Consider an elastic layer of thickness h with a circular cylindrical hole of radius a. The cylindrical coordinate system r, θ, z is used, r being the radial coordinate and z being the coordinate along the axis of symmetry, as shown in Fig. 1. The layer is resting on a rigid foundation in such a way that zero shear stress and zero normal displacement exists at the interface.

An axisymmetric radial displacement is imposed on the cylindrical boundary which varies linearly in the z-direction. This imposed deformation, shown in Fig. 2, gives rise to axially-symmetric displacements and stresses throughout the layer.

The problem shown in Fig. 3 represents an infinite free plate of thickness $2h$ with a circular cylindrical hole. The plate has an axisymmetric radial displacement imposed on the cylindrical boundary which is also symmetric about its mid-plane. This type of problem, which could be of practical importance, is completely equivalent to the problem represented in Figs. 1 and 2.

The Navier Equations.

The Navier equations of elasticity in cylindrical

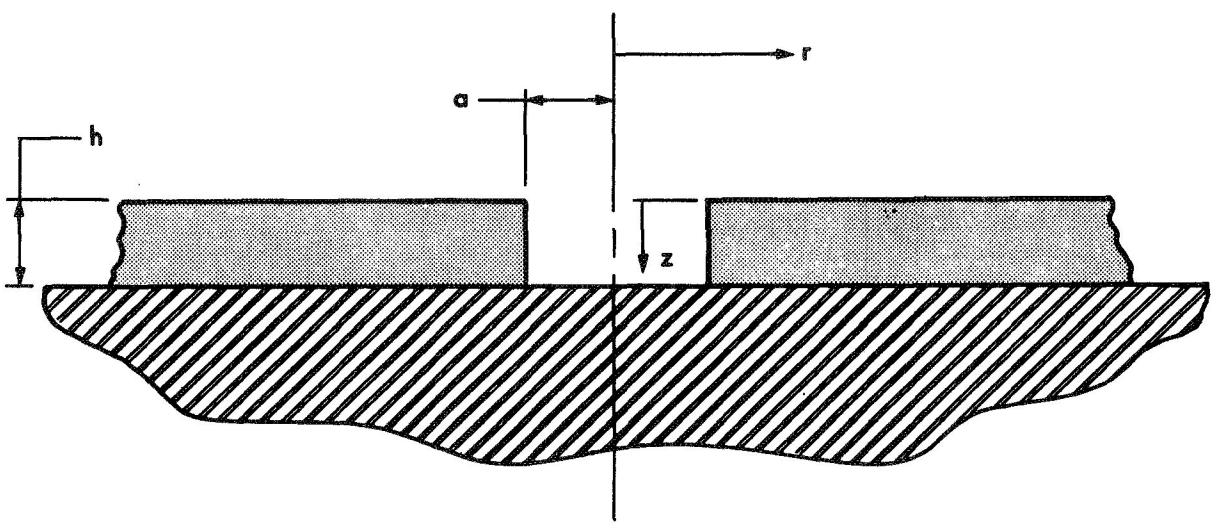

Figure 1. The elastic layer geometry and coordinate system.

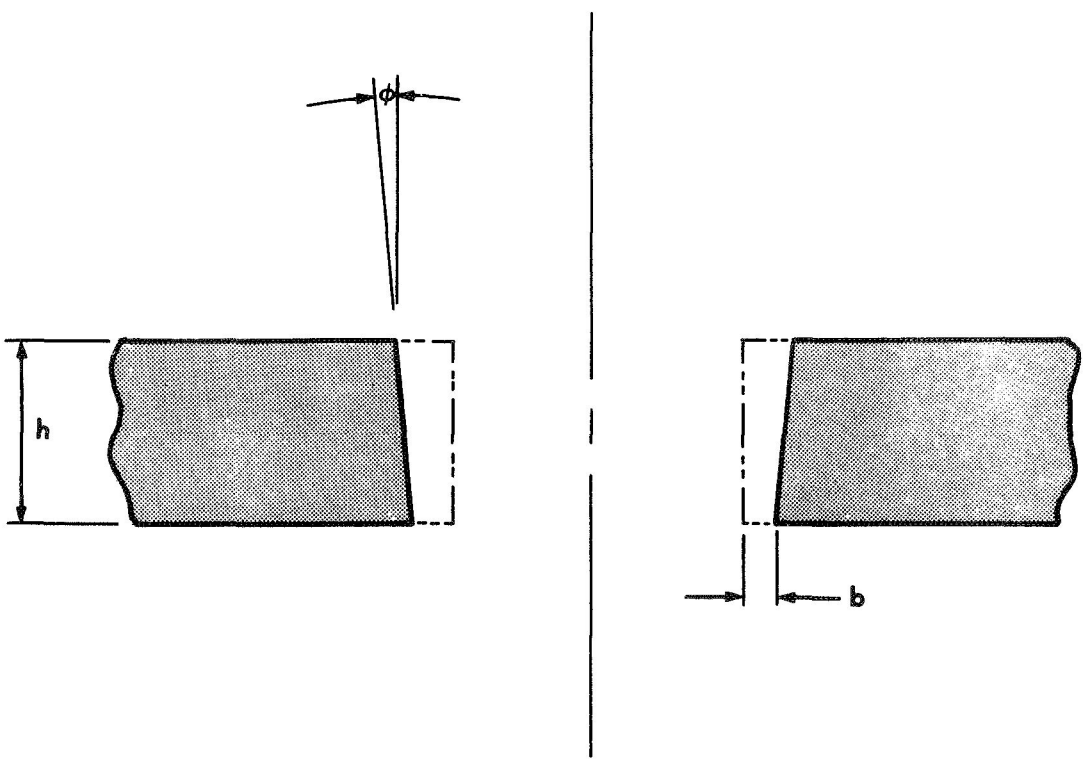

Figure 2. The imposed radial deformation of the layer.

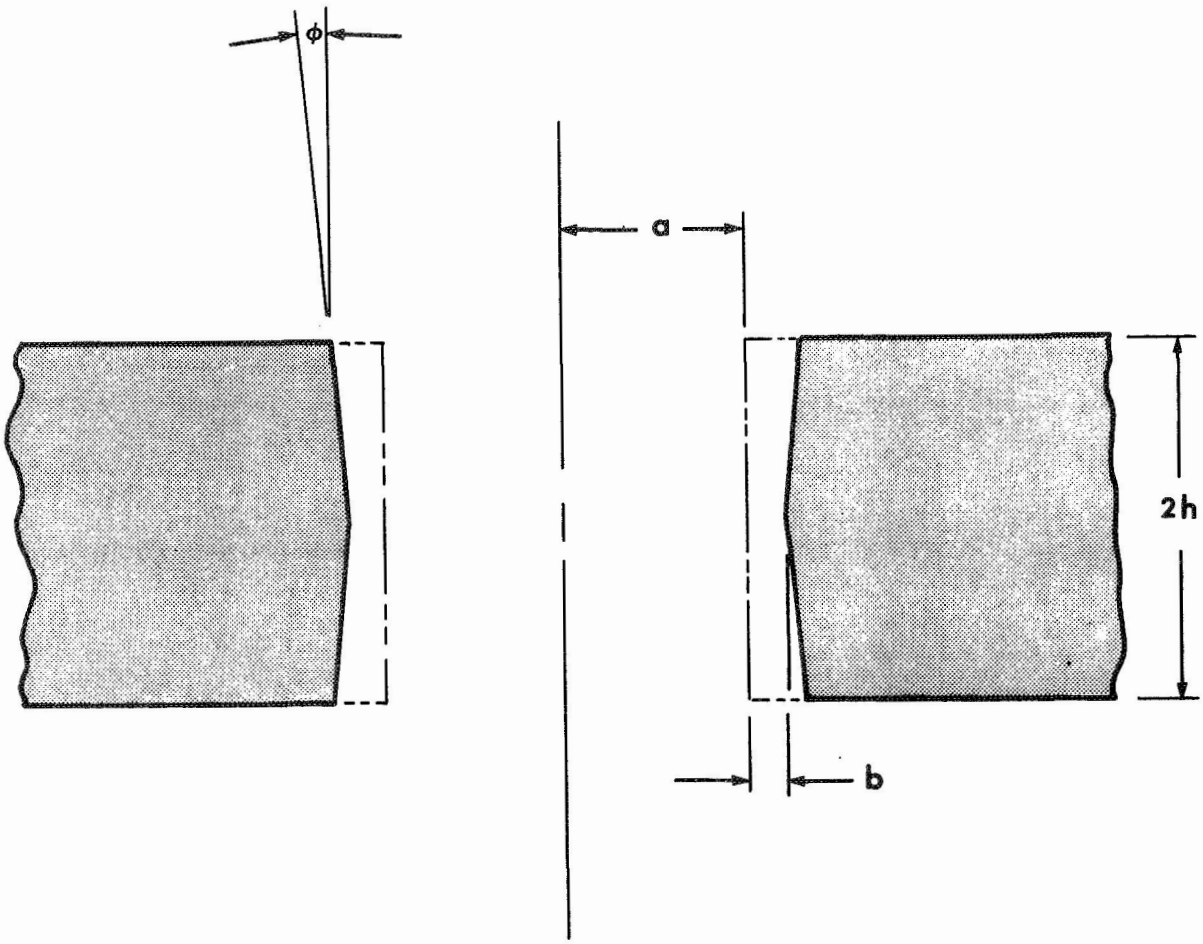

Figure 3. The equivalent problem.

coordinates for the case of axial symmetry are (see, for example, Reference 7):

$$2(1-\nu)\left(\frac{\partial^2 u}{\partial r^2}+\frac{1}{r}\frac{\partial u}{\partial r}-\frac{u}{r^2}\right)+(1-2\nu)\frac{\partial^2 u}{\partial z^2}+\frac{\partial^2 w}{\partial r\partial z}=0 \qquad (2.1)$$

$$(1-2\nu)\left(\frac{\partial^2 w}{\partial r^2}+\frac{1}{r}\frac{\partial w}{\partial r}\right)+2(1-\nu)\frac{\partial^2 w}{\partial z^2}+\frac{\partial}{\partial z}\left(\frac{\partial u}{\partial r}+\frac{u}{r}\right)=0 \qquad (2.2)$$

where u and w are radial and longitudinal displacements, respectively, and ν is Poisson's ratio.

Solution by Extended Hankel Transforms.

Following Scott and Miklowitz's work, Eqs. (2.1) and (2.2) will be solved by employing the $\mathcal{R}_0$ and $\mathcal{R}_1$ transforms defined by Eqs. (1.3) and (1.5) and Eqs. (1.4) and (1.6), respectively. Using the properties of the transforms given in Appendix A and applying the $\mathcal{R}_1$ transform to Eq. (2.1) and the $\mathcal{R}_0$ transform to Eq. (2.2), the following differential equations result:

$$-2(1-\nu)s^2\bar{u}+(1-2\nu)D^2\bar{u}-sD\bar{w}=\frac{4(1-\nu)}{\pi}u(a,z) \qquad (2.3)$$

$$-(1-2\nu)s^2\bar{w}+2(1-\nu)D^2\bar{w}+sD\bar{u}=\frac{-2(1-2\nu)}{s\pi}\frac{\partial w(a,z)}{\partial r}-\frac{z}{\pi s}\frac{\partial w(a,z)}{\partial z}, \qquad (2.4)$$

where $D\equiv\frac{d}{dz}$.

From Fig. 2, the imposed radial displacement is given

by the relation

$$u(a,z) = \delta + (h-z)\tan\phi \,. \tag{2.5}$$

Therefore,

$$\frac{\partial u(a,z)}{\partial z} = -\tan\phi \,. \tag{2.6}$$

The requirement that the cylindrical boundary be free of shear stress implies that

$$\frac{\partial w(a,z)}{\partial r} = -\frac{\partial u(a,z)}{\partial z} = \tan\phi \,. \tag{2.7}$$

Substituting Eqs. (2.5), (2.6) and (2.7) into Eqs. (2.3) and (2.4), one obtains:

$$-2(1-\nu)s^2\bar{u} + (1-2\nu)D^2\bar{u} - sD\bar{w} = \frac{4(1-\nu)}{\pi}\left[\delta + (h-z)\tan\phi\right] \tag{2.8}$$

$$-(1-2\nu)s^2\bar{w} + 2(1-\nu)D^2\bar{w} + sD\bar{u} = \frac{4\nu}{s\pi}\tan\phi \,. \tag{2.9}$$

It can be shown that these equations are equivalent to the following fourth order, uncoupled differential equations:

$$\left(D^4 - 2s^2D^2 + s^4\right)\bar{u} = \frac{2s^2}{\pi}\left(-\delta + (z-h)\tan\phi\right) \tag{2.10}$$

$$\left(D^4 - 2s^2D^2 + s^4\right)\bar{w} = \frac{2s}{\pi}\tan\phi \,. \tag{2.11}$$

The general solutions of Eqs. (2.10) and (2.11) are:

$$\bar{w} = B_1 e^{sz} + B_2 e^{-sz} + B_3 z e^{sz} + B_4 z e^{-sz} + \frac{2\pi m \sin\phi}{\pi s^3} \tag{2.12}$$

$$\bar{u} = C_1 e^{sz} + C_2 e^{-sz} + C_3 z e^{sz} + C_4 z e^{-sz} + \frac{2}{\pi s^3}\left[-b + (z-k)\pi m \sin\phi\right]. \tag{2.13}$$

Substituting Eqs. (2.12) and (2.13) into Eq. (2.8) gives the following relationships between the arbitrary constants:

$$B_1 = \frac{(3-\nu)C_3}{s} - C_1 \tag{2.14}$$

$$B_2 = \frac{(3-\nu)C_4}{s} + C_2 \tag{2.15}$$

$$B_3 = -C_3 \tag{2.16}$$

$$B_4 = C_4 . \tag{2.17}$$

Equation (2.12) now becomes

$$\bar{w} = \frac{(3-\nu)C_3 - sC_1}{s} e^{sz} + \frac{(3-\nu)C_4 + sC_2}{s} e^{-sz} - C_3 z e^{sz} + C_4 z e^{-sz} + \frac{2\pi m \sin\phi}{\pi s^3} . \tag{2.18}$$

Equations for Stresses.

The stress-strain relations for axial symmetry are (see, for example, Reference 8):

$$\sigma_z = (\lambda+2\mu)\frac{\partial w}{\partial z} + \lambda\left(\frac{\partial u}{\partial r} + \frac{u}{r}\right) \tag{2.19}$$

$$\sigma_r = (\lambda+2\mu)\frac{\partial u}{\partial r} + \lambda\left(\frac{u}{r} + \frac{\partial w}{\partial z}\right) \tag{2.20}$$

$$\sigma_\theta = (\lambda+2\mu)\frac{u}{r} + \lambda\left(\frac{\partial u}{\partial r} + \frac{\partial w}{\partial z}\right) \tag{2.21}$$

$$\sigma_{rz} = \mu\left[\frac{\partial u}{\partial z} + \frac{\partial w}{\partial r}\right], \tag{2.22}$$

where λ and μ are the Lame'constants.

Applying the $\mathcal{R}_0$transform to Eqs. (2.19), (2.20) and (2.21) and the $\mathcal{R}_1$transform to Eq. (2.22), one obtains

$$\overline{\sigma_z} = (\lambda+2\mu)D\bar{w} + \lambda\left(\frac{2}{\pi s}u(a,z) + s\bar{u}\right) \tag{2.23}$$

$$\overline{\sigma_r} = (\lambda+2\mu)\left[\frac{2}{\pi s}u(a,z) + s\bar{u} - \int_a^\infty u(r,z)R_0\,dr\right] + \lambda\left[D\bar{w} + \int_a^\infty u(r,z)R_0\,dr\right] \tag{2.24}$$

$$\overline{\sigma_\theta} = (\lambda+2\mu)\left[\int_a^\infty u(r,z)R_0\,dr\right] + \lambda\left[\frac{2}{\pi s}u(a,z) - \int_a^\infty u(r,z)R_0\,dr\right] \tag{2.25}$$

$$\overline{\sigma_{rz}} = \mu\left[D\bar{u} - s\bar{w}\right]. \tag{2.26}$$

Equations (2.24) and (2.25) are not in a useful form and, therefore, Eqs. (2.20) and (2.21) do not possess suitable transforms. Radial and circumferential stresses must be obtained from a method other than direct transformation of their respective stress-strain relations. Using the integral expressions for $u(r,z)$ and $w(r,z)$ and Eqs. (2.20) and (2.21), one obtains:

$$\sigma_r = (\lambda+2\mu)\frac{\partial}{\partial r}\int_0^\infty \frac{s\,\bar{u}(s,z)\,R_1\,ds}{J_1^2(as)+Y_1^2(as)} + \lambda\frac{1}{r}\int_0^\infty \frac{s\,\bar{u}(s,z)\,R_1\,ds}{J_1^2(as)+Y_1^2(as)} + \lambda\frac{\partial}{\partial z}\int_0^\infty \frac{s\,\bar{w}(s,z)\,R_0\,ds}{J_1^2(as)+Y_1^2(as)} \tag{2.27}$$

$$\sigma_\theta = (\lambda+2\mu)\frac{1}{r}\int_0^\infty \frac{s\,\bar{u}(s,z)\,R_1\,ds}{J_1^2(as)+Y_1^2(as)} + \lambda\frac{\partial}{\partial r}\int_0^\infty \frac{s\,\bar{u}(s,z)\,R_1\,ds}{J_1^2(as)+Y_1^2(as)} + \lambda\frac{\partial}{\partial z}\int_0^\infty \frac{s\,\bar{w}(s,z)\,R_0\,ds}{J_1^2(as)+Y_1^2(as)}\,. \tag{2.28}$$

If the following three conditions are satisfied, the order of integration and differentiation may be interchanged (see, for example, Reference 9):

(i) the integrands are continuous

(ii) the given integral exists

(iii) the resulting integral is uniformly convergent.

It can be shown that these conditions are satisfied. The first two conditions are obvious and the third condition requires knowledge of the arbitrary constants in Eqs. (2.13) and (2.18) which are determined in a later section.

Interchanging the order of integration and differentiation and performing the necessary operations, Eqs. (2.27) and (2.28) become:

$$\sigma_{\tau}(\tau,z) = (\lambda+2\mu)\int_0^{\infty} \frac{f_1(s,z)\, R_0\, ds}{J_1^2(as)+Y_1^2(as)} + \lambda\int_0^{\infty} \frac{f_2(s,z)\, R_0\, ds}{J_1^2(as)+Y_1^2(as)} - \frac{2\mu}{r}\int_0^{\infty} \frac{s\,\bar{u}(s,z)\, R_1\, ds}{J_1^2(as)+Y_1^2(as)} \tag{2.29}$$

$$\sigma_{\theta}(\tau,z) = \lambda\int_0^{\infty} \frac{[f_1(s,z)+f_2(s,z)]\, R_0\, ds}{J_1^2(as)+Y_1^2(as)} + \frac{2\mu}{r}\int_0^{\infty} \frac{s\,\bar{u}(s,z)\, R_1\, ds}{J_1^2(as)+Y_1^2(as)}, \tag{2.30}$$

where $$f_1(s,z) = s^2\left[e^{sz}(c_1+zc_3)+e^{-sz}(c_2+zc_4)\right] \tag{2.31}$$

$$f_2(s,z) = s\{e^{sz}[(2(1-2\nu)-sz)c_3 - sc_1] + e^{-sz}[(-2(1-2\nu)-sz)c_4 - sc_2]\}. \tag{2.32}$$

Completing the operations as prescribed by Eqs. (2.23) and (2.26), the following expressions are obtained for transformed longitudinal and shear stresses:

$$\overline{\sigma_z} = \frac{\lambda}{\nu}\left\{ e^{sz}\left[\left(2-6\nu+4\nu^2-sz(1-2\nu)\right)C_3 - s(1-2\nu)C_1\right] - e^{-sz}\left[\left(2-6\nu+4\nu^2+ sz(1-2\nu)\right)C_4 + s(1-2\nu)C_2\right]\right\} \tag{2.33}$$

$$\overline{\sigma_{rz}} = 2\mu\left\{ e^{sz}\left[sC_1 - (1-2\nu-sz)C_3\right] - e^{-sz}\left[sC_2 + (1-2\nu+sz)C_4\right]\right\}. \tag{2.34}$$

The longitudinal and shear stresses can now be obtained by inverting Eqs. (2.33) and (2.34). Using Eqs. (1.5) and (1.6), one has:

$$\sigma_z(r,z) = \int_0^\infty \frac{s\,\overline{\sigma_z}(s,z)\,R_0\,ds}{J_1^2(as)+Y_1^2(as)} \tag{2.35}$$

$$\sigma_{rz}(r,z) = \int_0^\infty \frac{s\,\overline{\sigma_{rz}}(s,z)\,R_1\,ds}{J_1^2(as)+Y_1^2(as)}. \tag{2.36}$$

Determination of Arbitrary Constants.

From the statement of the problem, the following boundary conditions can be deduced (refer to Fig. 1):

$$\sigma_z(r,0) = 0 \tag{2.37}$$

$$\sigma_{rz}(r,0) = 0 \tag{2.38}$$

$$\sigma_{rz}(r,h) = 0 \tag{2.39}$$

$$w(r,h) = 0 . \tag{2.40}$$

Applying the $\mathcal{R}_0$ transform to both sides of Eqs. (2.37) and (2.40) and the $\mathcal{R}_1$ transform to both sides of Eqs. (2.38) and (2.39), one obtains for the transformed boundary conditions:

$$\overline{\sigma_z}(s,0) = 0 \tag{2.41}$$

$$\overline{\sigma_{rz}}(s,0) = 0 \tag{2.42}$$

$$\overline{\sigma_{rz}}(s,h) = 0 \tag{2.43}$$

$$\overline{w}(s,h) = 0 . \tag{2.44}$$

Substituting these boundary conditions into Eqs. (2.18), (2.33) and (2.34), the following equations in C_1, C_2, C_3 and C_4 result:

$$-sC_1 - sC_2 + 2(1-\nu)C_3 - 2(1-\nu)C_4 = 0 \qquad (2.45)$$

$$sC_1 - sC_2 - (1-2\nu)C_3 - (1-2\nu)C_4 = 0 \qquad (2.46)$$

$$se^{sh}C_1 - se^{-sh}C_2 - (1-2\nu-sh)e^{sh}C_3 - (1-2\nu+sh)e^{-sh}C_4 = 0 \qquad (2.47)$$

$$e^{sh}C_1 - e^{-sh}C_2 - \frac{(3-4\nu-sh)}{s}e^{sh}C_3 - \frac{(3-4\nu+sh)}{s}e^{-sh}C_4 = -\frac{2\tan\phi}{\pi s^3} \qquad (2.48)$$

Equations (2.45) through (2.48) have the solution:

$$C_1 = \frac{\tan\phi\{e^{sh}[(1-2\nu)-sh] + e^{-sh}[(1-2\nu)+sh(3-4\nu)]\}}{\pi s^3(1-\nu)(-4sh - e^{2sh} + e^{-2sh})} \qquad (2.49)$$

$$C_2 = \frac{\tan\phi\{e^{sh}[-(1-2\nu)-sh(3-4\nu)] + e^{-sh}[(1-2\nu)+sh]\}}{\pi s^3(1-\nu)(-4sh - e^{2sh} + e^{-2sh})} \qquad (2.50)$$

$$C_3 = \frac{\tan\phi\{e^{sh} - (1-2sh)e^{-sh}\}}{\pi s^2(1-\nu)(-4sh - e^{2sh} + e^{-2sh})} \qquad (2.51)$$

$$C_4 = \frac{\tan\phi\{(1-2sh)e^{sh} - e^{-sh}\}}{\pi s^2(1-\nu)(-4sh - e^{2sh} + e^{-2sh})} . \qquad (2.52)$$

Special Case, $\phi = 0$.

To reduce this problem to that worked by Scott and Miklowitz, i.e., one where the imposed radial displacement is constant with respect to z, ϕ is merely set equal to zero. This causes the arbitrary constants to vanish and Eqs. (2.13), (2.18), (2.29), (2.30), (2.33) and (2.34) become:

$$\overline{u}(r,s) = -\frac{2b}{\pi s^2} \qquad (2.53)$$

$$\overline{w}(r;s) = 0 \tag{2.54}$$

$$\sigma_r(r,z) = -\frac{2\mu}{r}\int_0^\infty \frac{s\,\bar{u}(s,z)\,R_1\,ds}{J_1^2(as)+Y_1^2(as)} \tag{2.55}$$

$$\sigma_\theta(r,z) = \frac{2\mu}{r}\int_0^\infty \frac{s\,\bar{u}(s,z)\,R_1\,ds}{J_1^2(as)+Y_1^2(as)} \tag{2.56}$$

$$\overline{\sigma_z}(r;s) = 0 \tag{2.57}$$

$$\overline{\sigma_{rz}}(r;s) = 0\,. \tag{2.58}$$

Using the property from Appendix A that

$$\int_0^\infty \frac{R_1(0,s,r)\,ds}{s\left[J_1^2(as)+Y_1^2(as)\right]} = -\frac{\pi a}{2r}\,,$$

the above equations can be summarized as:

$$w(r,z) = \sigma_z(r,z) = \sigma_{rz}(r,z) = 0 \tag{2.59}$$

$$u(r) = \frac{ba}{r} \tag{2.60}$$

$$\sigma_r(r) = -\frac{2\mu ba}{r^2} \tag{2.61}$$

$$\sigma_\theta(r) = \frac{2\mu ba}{r^2}\,. \tag{2.62}$$

The expressions for u and w agree with the plotted data ("long-time solution") by Scott and Miklowitz. In addition, the expressions for displacements and stresses agree exactly with Lame's solution for a thick-walled cylinder (see, for example, Reference 10) when the outer radius is infinite.

Nondimensionalized Equations.

The equations for stresses and displacements can be nondimensionalized by introducing the following dimensionless variables: $\alpha = a/h$, $\beta = b/h$, $\eta = sh$, $\rho = r/h$ and $\xi = z/h$. With these substitutions, Eqs. (2.5), (2.6), (2.35), (2.36), (2.29) and (2.30) take the nondimensional forms:

$$\frac{u(\rho,\xi)}{h} = \int_0^\infty \frac{\eta\,\bar{u}(\eta,\xi)\,R_1(\alpha,\rho,\eta)\,d\eta}{J_1^2(\alpha\eta)+Y_1^2(\alpha\eta)} \tag{2.63}$$

$$\frac{w(\rho,\xi)}{h} = \int_0^\infty \frac{\eta\,\bar{w}(\eta,\xi)\,R_0(\alpha,\rho,\eta)\,d\eta}{J_1^2(\alpha\eta)+Y_1^2(\alpha\eta)} \tag{2.64}$$

$$\frac{\sigma_z(\rho,\xi)}{E} = \int_0^\infty \frac{\eta\,\bar{\sigma}_z(\eta,\xi)\,R_0(\alpha,\rho,\eta)\,d\eta}{J_1^2(\alpha\eta)+Y_1^2(\alpha\eta)} \tag{2.65}$$

$$\frac{\sigma_{rz}(\rho,\xi)}{E} = \int_0^\infty \frac{\eta\,\bar{\sigma}_{rz}(\eta,\xi)\,R_0(\alpha,\rho,\eta)\,d\eta}{J_1^2(\alpha\eta)+Y_1^2(\alpha\eta)} \tag{2.66}$$

$$\frac{\sigma_r(r,z)}{E} = \frac{(1-\nu)}{(1+\nu)(1-2\nu)} \int_0^\infty \frac{f_1(\eta,\xi)\, R_0(\alpha,\beta,\eta)\, d\eta}{J_1^2(\alpha\eta) + Y_1^2(\alpha\eta)} +$$

$$+ \frac{\nu}{(1+\nu)(1-2\nu)} \int_0^\infty \frac{f_2(\eta,\xi)\, R_0(\alpha,\beta,\eta)\, d\eta}{J_1^2(\alpha\eta) + Y_1^2(\alpha\eta)} -$$

$$- \frac{\left[\frac{u(r,z)}{z}\right]}{\rho(1-\nu)} \qquad (2.67)$$

$$\frac{\sigma_\theta(r,z)}{E} = \frac{\nu}{(1+\nu)(1-2\nu)} \int_0^\infty \frac{[f_1(\xi,\eta) + f_2(\xi,\eta)]\, R_0(\alpha,\beta,\eta)\, d\eta}{J_1^2(\alpha\eta) + Y_1^2(\alpha\eta)}$$

$$+ \frac{\left[\frac{w(r,z)}{z}\right]}{\rho(1-\nu)} \,, \qquad (2.68)$$

where

$$\bar{u}(\xi,\eta) = C_1 e^{\xi\eta} + C_2 e^{-\xi\eta} + C_3 \xi e^{\xi\eta} +$$

$$+ C_4 \xi e^{\xi\eta} + \frac{2\xi \tan\phi}{\pi\eta^2} - \frac{2}{\pi\eta^2}(\beta + \tan\phi)$$

$$\bar{w}(\xi,\eta) = \left[\frac{(3-4\nu)C_3}{\eta} - C_1\right] e^{\xi\eta} +$$

$$+ \left[\frac{(3-4\nu)C_4}{\eta} + C_2\right] e^{-\xi\eta} - C_3 \xi e^{\xi\eta}$$

$$+ C_4 \xi e^{-\xi\eta} + \frac{2\tan\phi}{\pi\eta^3}$$

$$\bar{\sigma}_z(\xi,\eta) = \frac{\lambda}{2}\Big\{ e^{\xi\eta}\big[(2-6\nu+4\nu^2-(1-2\nu)\xi\eta)C_3 -$$

$$- \eta(1-2\nu)C_1\big] - e^{-\xi\eta}\big[(2-6\nu+4\nu^2 +$$

$$+ (1-2\nu)\xi\eta)C_4 + \eta(1-2\nu)C_2\big]\Big\}$$

$$\overline{\sigma_{rz}}(\xi,\eta) = 2\mu\{ e^{\xi\eta}[\eta C_1 - (1-2\nu-\xi\eta)C_3] - e^{-\xi\eta}[\eta C_2 + (1-2\nu+\xi\eta)C_4]$$

$$C_1 = \frac{\tan\phi\{ e^{\eta}[(1-2\nu)-\eta(3-4\nu)] + e^{-\eta}[(1-2\nu)+\eta]\}}{\pi\eta^3(1-\nu)(-4\eta - e^{2\eta} + e^{-2\eta})}$$

$$C_2 = \frac{\tan\phi\{ e^{\eta}[-(1-2\nu)-\eta(3-4\nu)] + e^{-\eta}[(1-2\nu)+\eta]\}}{\pi\eta^3(1-\nu)(-4\eta - e^{2\eta} + e^{-2\eta})}$$

$$C_3 = \frac{\tan\phi\{ e^{\eta} - (1-2\eta)e^{-\eta}\}}{\pi\eta^2(1-\nu)(-4\eta - e^{2\eta} + e^{-2\eta})}$$

$$C_4 = \frac{\tan\phi\{ e^{\eta}(1+2\eta) - e^{-\eta}\}}{\pi\eta^2(1-\nu)(-4\eta - e^{2\eta} + e^{-2\eta})}$$

$$f_1(\xi,\eta) = \eta^2\{ e^{\xi\eta}(C_1 + \xi C_3) + e^{-\xi\eta}(C_2 + \xi C_4)\}$$

$$f_2(\xi,\eta) = \eta\{ e^{\xi\eta}[(2(1-2\nu)-\xi\eta)C_3 - \eta C_1] + e^{-\xi\eta}[(-2(1-2\nu)-\xi\eta)C_4 - \eta C_2]\}$$

$$R_0(\alpha,\rho,\eta) = J_0(\rho\eta)Y_1(\alpha\eta) - J_1(\alpha\eta)Y_0(\rho\eta)$$

$$R_1(\alpha,\rho,\eta) = J_1(\rho\eta)Y_1(\alpha\eta) - J_1(\alpha\eta)Y_1(\rho\eta).$$

Singularity at $r = a$, $z = h$.

It can be shown that a singular point occurs at $r = a$, $z = h$. Radial and longitudinal displacements and shear stress have imposed boundary conditions at this point, however, radial, longitudinal and circumferential stresses increase without bound.

For large arguments of the independent variable s, the functions $\overline{\sigma_z}$, f_1 and f_2 (Reference Eqs. 2.31, 2.32 and 2.33) can be shown to approach $\frac{1}{s}$ for $z = h$. Also, for large arguments of the independent variable s and for $r = a$, the following condition holds:

$$\lim_{s \to \infty} \frac{R_o(s,a,a)}{J_1^2(sa) + Y_1^2(sa)} = \text{CONSTANT}$$

Applying these two properties to Eqs. (2.29), (2.30) and (2.35), it can be shown the inversion integrals for the radial, longitudinal and circumferential stresses fail to exist.

CHAPTER III

NUMERICAL EVALUATION OF INVERSE TRANSFORMS

The numerical inversion of Eqs. (2.63) through (2.68) is accomplished using a technique developed by Longman [11]. Longman's method is based on Euler's transformation of a convergent, alternating series[12]. A brief explanation of the method is given below.

According to Euler's transformation, an infinite series

$$V_0 - V_1 + V_2 - V_3 + V_4 - \cdots ,$$

where

$$V_n > 0 , \quad V_{n+1} < V_n , \quad \text{FOR ALL } n ,$$

and

$$\Delta V_n = V_{n+1} - V_n , \quad \Delta^{i+1} V_n = \Delta^i V_{n+1} - \Delta^i V_n ,$$

can be expressed as

$$\sum_{n=0}^{\infty} (-1)^n V_n = \frac{1}{2} V_0 - \frac{1}{4} \Delta V_0 + \frac{1}{8} \Delta^2 V_0 - \cdots . \tag{3.1}$$

Consider a function which oscillates about zero in such a way that the integral over each half-cycle is smaller in absolute value than that over the preceding half-cycle. The infinite integral of this function can be represented as an infinite alternating series where the ith term is the integral over the ith half-cycle. Applying Euler's transformation to this series gives an accurate answer for a relative short interval of integration. The degree of accuracy is illustrated in Longman's paper [11].

To use this method, it is necessary to determine the roots of the inversion integrands. The equations from which the roots are computed, based on asymtotic approximations of the Bessel functions, are derived in Appendix B.

For large values of the radial parameter, successive magnitudes of the half-cycle integrations were found to initially increase. The largest magnitude existed for the third half-cycle. Using a series of seven terms (integrals of the first seven half-cycles) to approximate the integral and applying Euler's transformation to the last five terms, gives for the value of the integral

$$I \cong V_1 + V_2 \pm \left[\frac{1}{2}V_3 - \frac{1}{4}\Delta V_3 + \frac{1}{8}\Delta^2 V_3 - \frac{1}{16}\Delta^3 V_3 + \frac{1}{32}\Delta^4 V_3\right] \qquad (3.2)$$

In this form, each term retains its computed sign and the sign of the bracketed terms is the same as that of V_3.

Plots of the inversion kernels, K_0 and K_1, as functions of radial parameter are presented in Appendix C. Additionally, selected plots of various inversion integrands are presented.

All numerical computations were accomplished by use of the Univac 1108. The method of integration was Simpson's 3/8 Rule. Routines for integration and evaluation of Bessel functions were obtained from the Univac library program, "MATH-PACK".

CHAPTER IV

RESULTS

Figures 4 through 17 are plots of the nondimensional displacements and stresses as functions of the radial parameter r/a for three different values of the axial coordinate Z. Figures 4 through 7 are for the upper surface ($Z = \zeta = 0$), Figs. 8 through 13 for the mid-plane ($Z = h/2$, $\zeta = .5$) and Figs. 14 through 17 for the lower plane ($Z = h$, $\zeta = 1.0$). Each Figure has two curves; one corresponding to α equal one and the other for α equal two. The dimensionless parameter α is defined as the ratio of hole radius to layer thickness. For all computations, the values $\nu = .3$, $\beta = .01$ and $\phi = .020833$ were used. Figures 18 and 19 are sketches of the deformed state (heavy lines) superimposed on the undeformed state (light lines) for $\alpha = 1.0$ and $\alpha = 2.0$, respectively.

Figures 4, 8 and 14 are curves for nondimensional radial displacements, u/h. Figures 4 and 8 are curves for the upper surface and mid-plane, respectively. As shown, the radial displacements are smooth, monotonically decreasing functions. The curves in Fig. 14 give the radial displacement of the lower surface. The curves exhibit an initial increase, reach their maximum values at r/a slightly greater than unity, and approach zero in the same smooth manner as the curves of Figs. 4 and 8.

The graphs for nondimensional longitudinal displacements, w/h, are shown in Figs. 5 and 9 for the upper surface and mid-plane, respectively. Each curve shows negative values of displacement (upward) at $r = a$. With increasing r/a, each curve rapidly decreases in magnitude to zero, becomes positive and then approaches zero asymtotically.

Figures 6 and 7 represent the nondimensional radial and circumferential stresses, σ_r/E and σ_θ/E, respectively, on the upper surface. It can be seen that the radial stresses are compressive and rapidly approach zero with r/a. The circumferential stresses are tensile and approach zero in an equally rapid manner. As one would expect, the radial stresses have the larger maximum values (at $r = a$).

Figures 10, 11, 12 and 13 are curves of the nondimensional radial, longitudinal, circumferential and shear stresses, respectively, on the mid-plane. Radial and circumferential stresses behave as they did on the upper surface and are approximately equal in magnitude. The longitudinal stress, σ_z/E, is seen to rapidly decrease in magnitude. The stress is initially tensile, becomes compressive and then approaches zero. The curve for shear stress, σ_{rz}/E, shows a rapid variation in magnitude. The value of shear stress is initially zero, but quickly reaches a maximum and then approaches zero.

Figures 15, 16 and 17 are curves for nondimensional radial, longitudinal and circumferential stresses, respectively. Each curve exhibits a singularity at $r = a$. This feature will

be discussed later. The longitudinal stress is shown as initially tensile. A rapid change from tensile to compressive stress occurs with a subsequent tendency to zero. The curve of radial stress exhibits the same general properties. The curve for circumferential stress is monotonically decreasing and, with the exception of the singularity, possesses the same basic properties as the other curves of circumferential stresses.

Figures 18 and 19 depict the deformed shapes of the layer for the two cases of $\alpha = 1$ and $\alpha = 2$, respectively. It can be seen that longitudinal displacement becomes insignificant with respect to radial displacement for increasing values of r/a.

The singularity that exists at $r = a, z = h$ can be best understood by considering the imposed boundary conditions. The shear stress on the cylindrical boundary is prescribed as zero. This fact, as shown by Eq. (2.7), requires the following condition:

$$\frac{\partial w(a,z)}{\partial r} = \tan \phi .$$

On the lower surface, the longitudinal displacement, w, is forced to be zero. This constraint on normal displacement gives rise to the following condition.

$$\frac{\partial w(r,h)}{\partial r} = 0 .$$

From these two equations, it can be seen that at $r = a$,

$z = h$, inconsistent constraints result which will force a singularity.

Curves for stresses and displacements are plotted using computed data over the range $1.05 \leq r/a \leq 3.5$. Below $r/a = 1.05$, significant error was introduced because of truncation in the evaluation of the infinite integrals. The number of roots of the integrands that could be used in the integration technique described in Chapter III became limited due to their magnitudes. The roots became sufficiently large and caused computational overflow in the computer. As r approaches a, the roots of each integrand increases without bound. At values of r/a close to unity, the first several roots take on very large values. Reference is made to Appendices B and C where the equations for computing the roots and curves showing integrand dependence on r, respectively, are shown. With the exception of stresses at the singular point, all curves were extrapolated to $r/a = 1.0$. The extrapolation provided excellent results for radial displacements, u/h, Figs. 4, 8 and 14, where the data at $r = a$ was known. Also, extrapolation of the curves for shear stress, σ_{rz}/E, Fig. 13, provided good results at $r = a$ where the shear stress was imposed as zero.

It is interesting to note two features which are contrary to what one might intuitively expect. From Figs. 15 and 16, it can be seen that radial and longitudinal stresses are tensile at $r = a$ ($z = h$). The longitudinal stress is tensile

because the surface of the cylindrical hole is negatively displaced (upward) but is constrained to be zero at the lower surface. This extension gives rise to positive strain and, therefore, tensile stress. The cylindrical boundary being displaced upward is attributed to the absence of shear stress on its surface. The radial stress is tensile because the larger radial displacement imposed on the upper portion of the layer attempts by shear to displace the lower portion farther than the boundary condition will allow. This also explains the odd shape of the radial displacement curve, Fig. 14, for the lower surface.

Reasonable accuracy was obtained in checking the computed data by use of the following stress-strain relation for the case of axial symmetry:

$$\frac{u}{r} = \frac{\sigma_\theta}{E} - \nu\left(\frac{\sigma_r}{E} + \frac{\sigma_z}{E}\right).$$

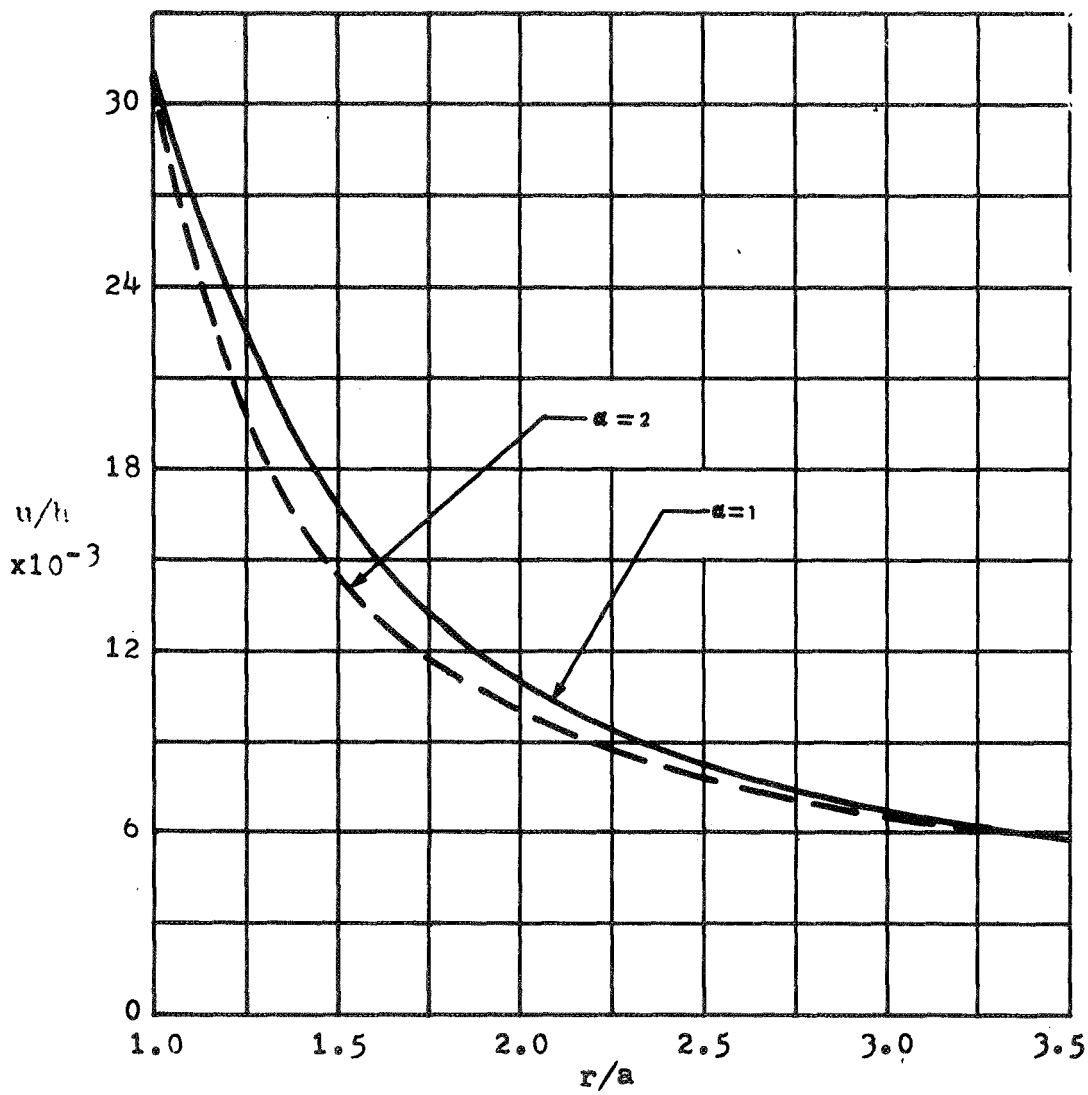

Figure 4. Nondimensional radial displacement as a function of radial coordinate.

$\zeta = 0 \qquad \beta = .01 \qquad \phi = .020833$

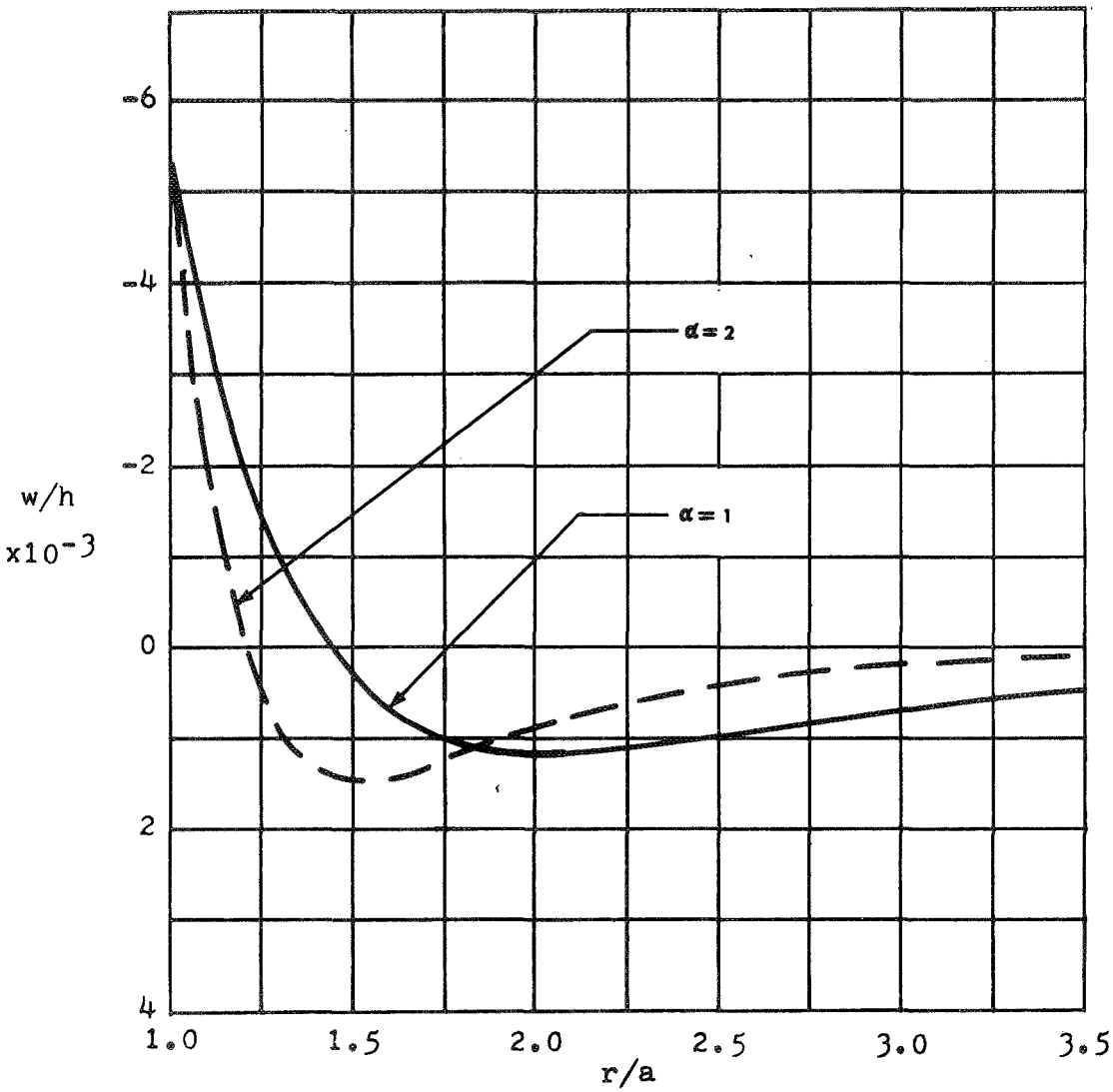

Figure 5. Nondimensional longitudinal displacement as a function of radial coordinate.

$\zeta = 0 \qquad \beta = .01 \qquad \phi = .020833$

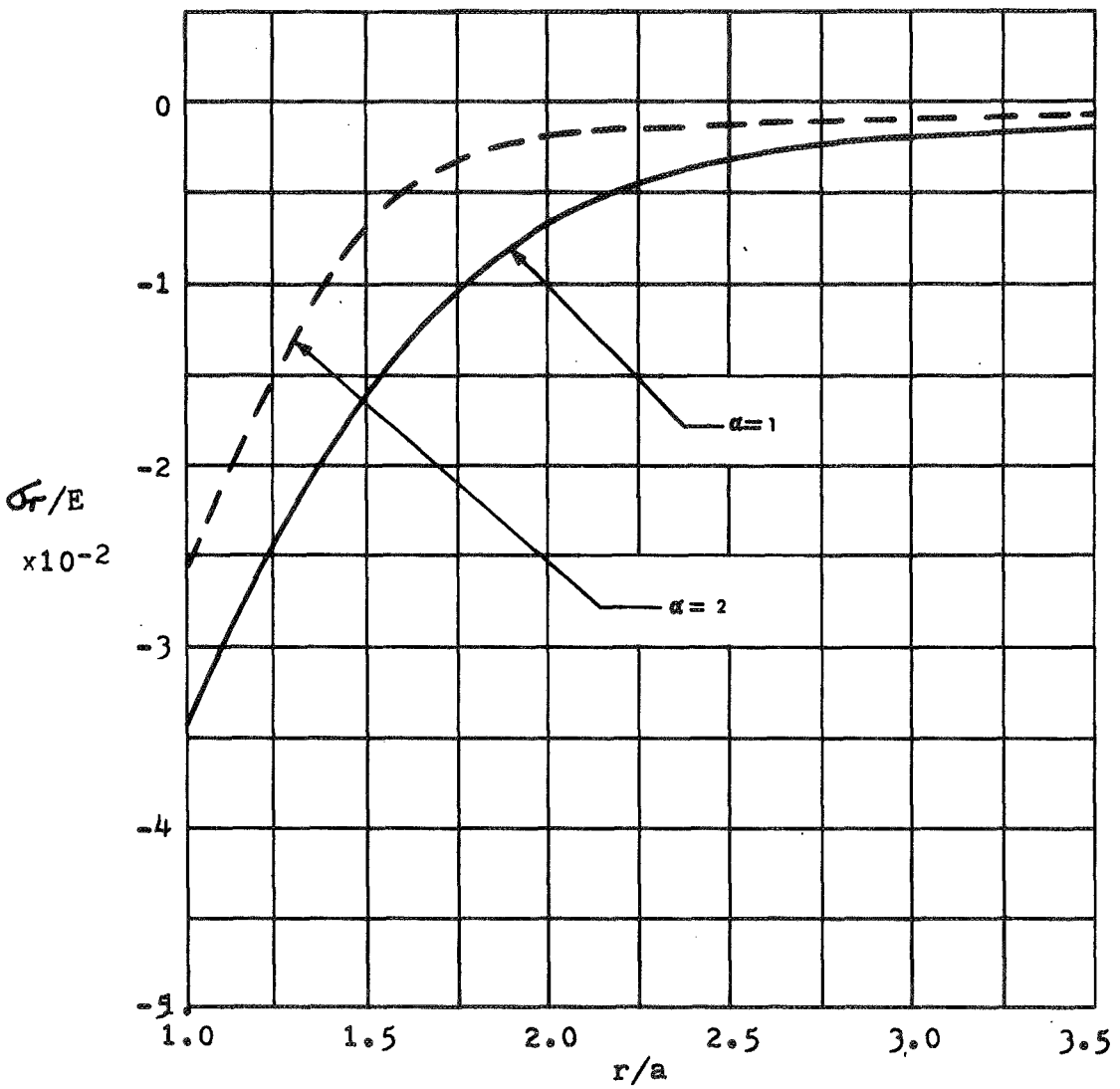

Figure 6. Nondimensional radial stress as a function of radial coordinate.

$\zeta = 0$ $\beta = .01$ $\phi = .020833$

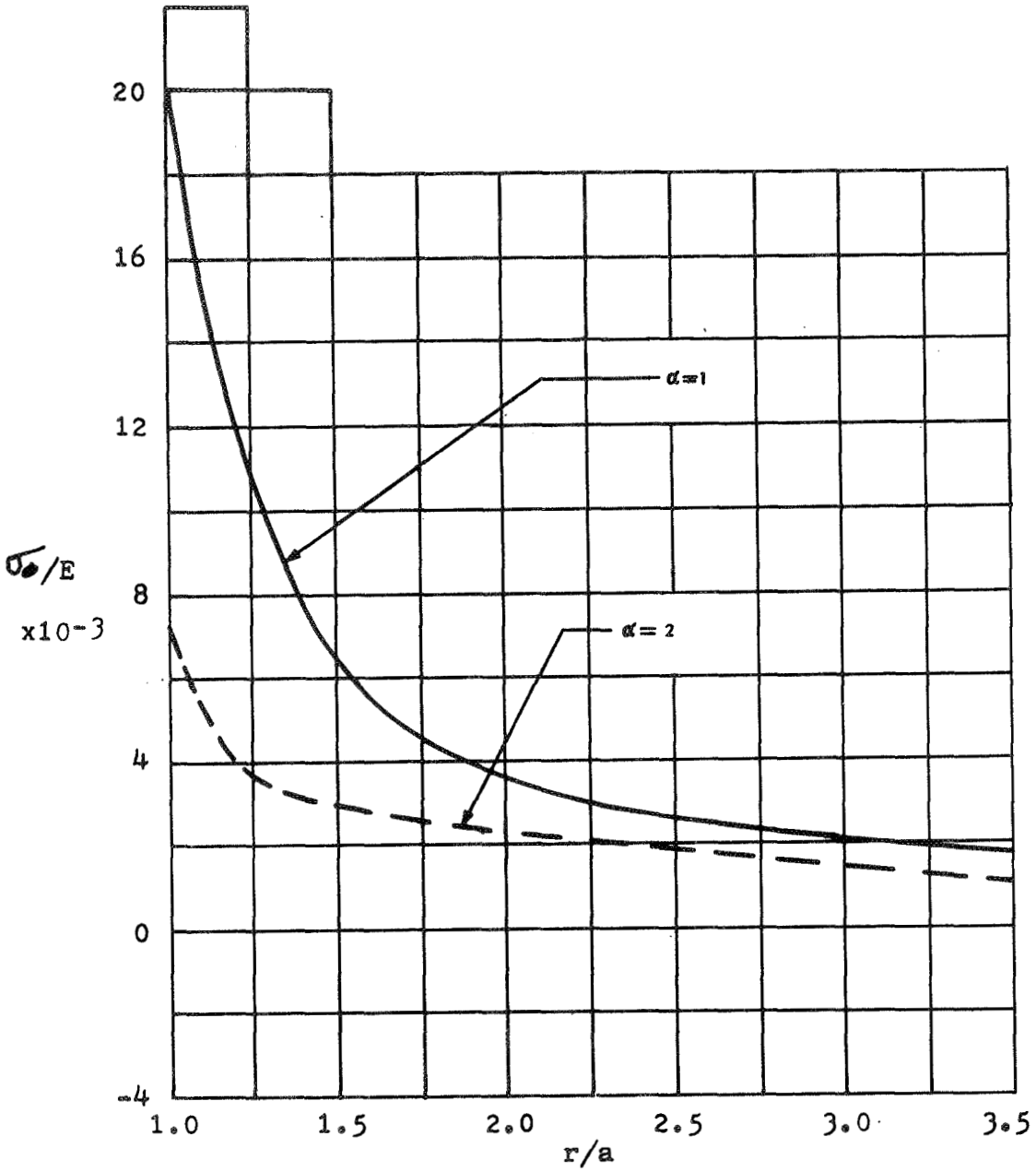

Figure 7. Nondimensional circumferential stress as a function of radial coordinate.

$\zeta = 0 \qquad \beta = .01 \qquad \Phi = .020833$

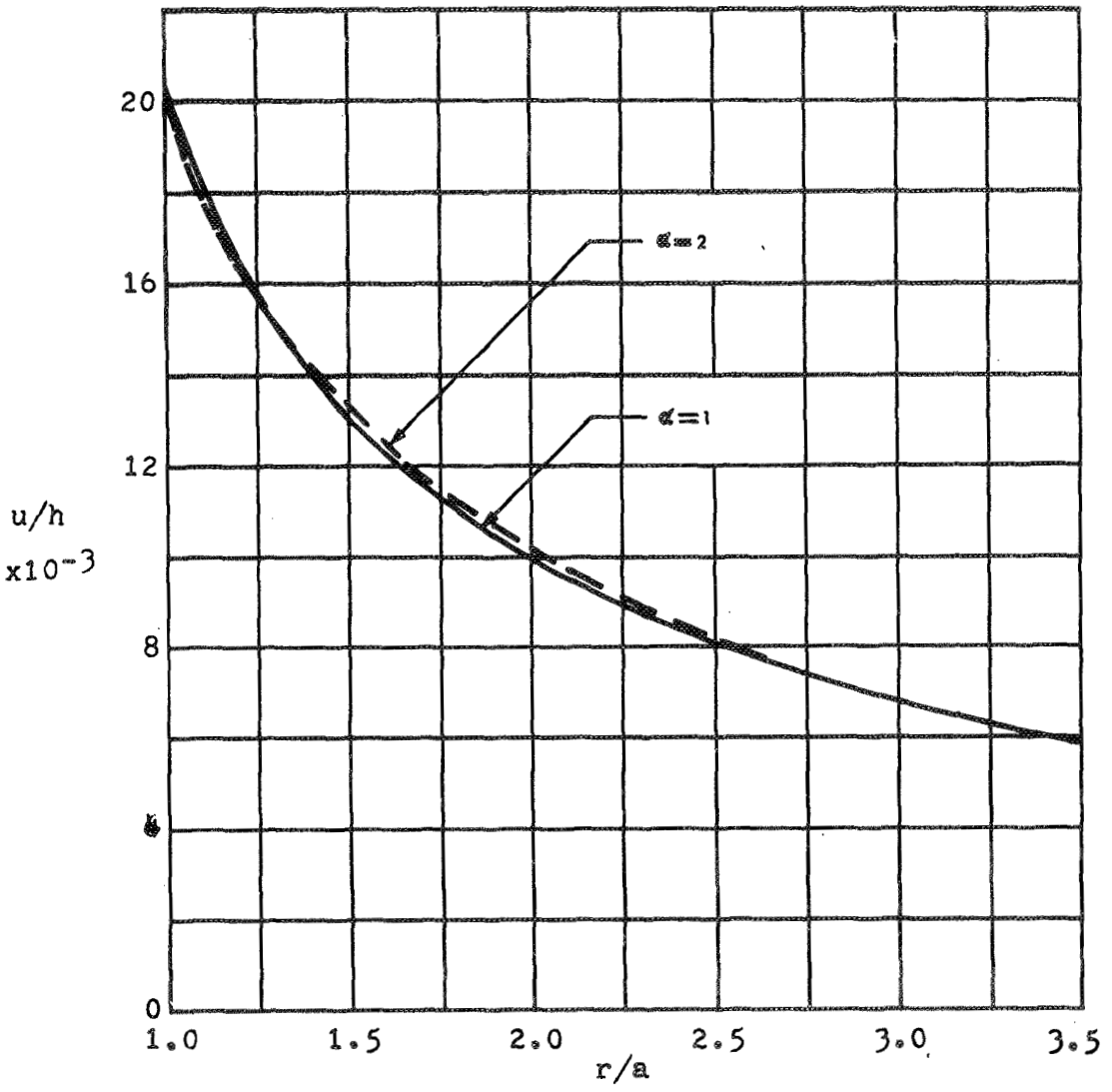

Figure 8. Nondimensional radial displacement as a function of radial coordinate.

$\zeta = .5 \quad \beta = .01 \quad \phi = .020833$

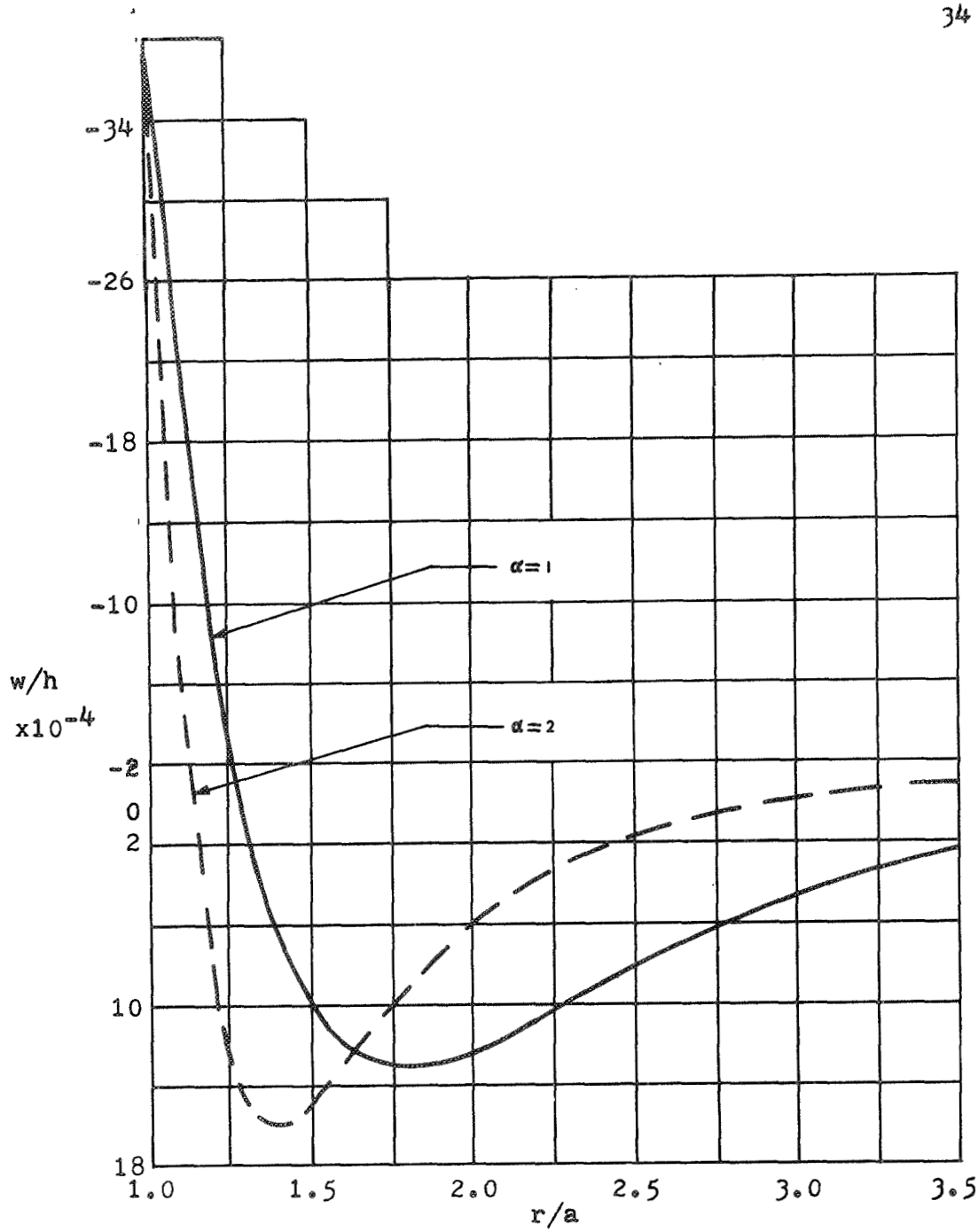

Figure 9. Nondimensional longitudinal displacement as a function of radial coordinate.

$\zeta = .5 \quad \beta = .01 \quad \phi = .020833$

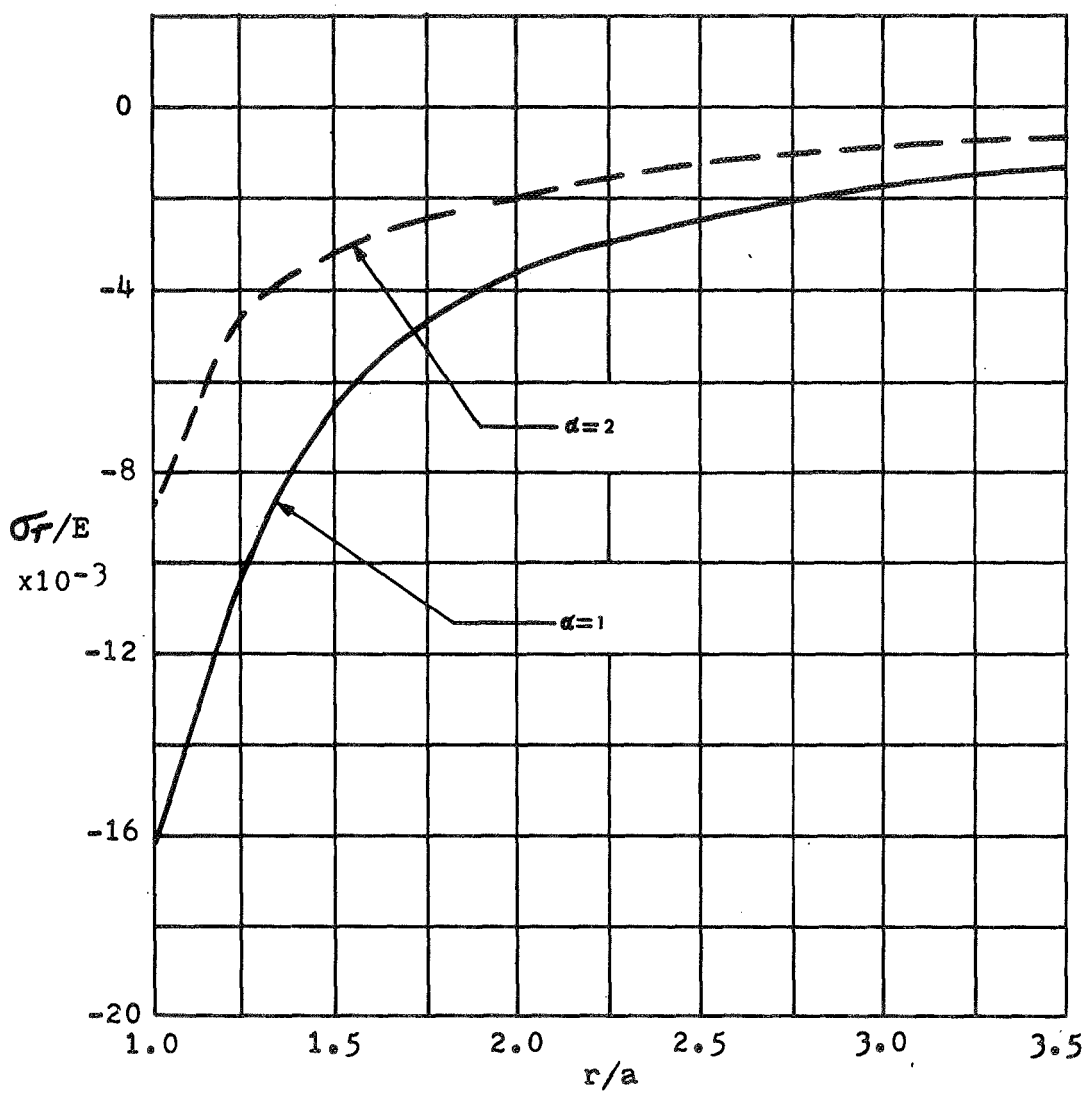

Figure 10. Nondimensional radial stress as a function of radial coordinate.

$\gamma = .5 \quad \beta = .01 \quad \phi = .020833$

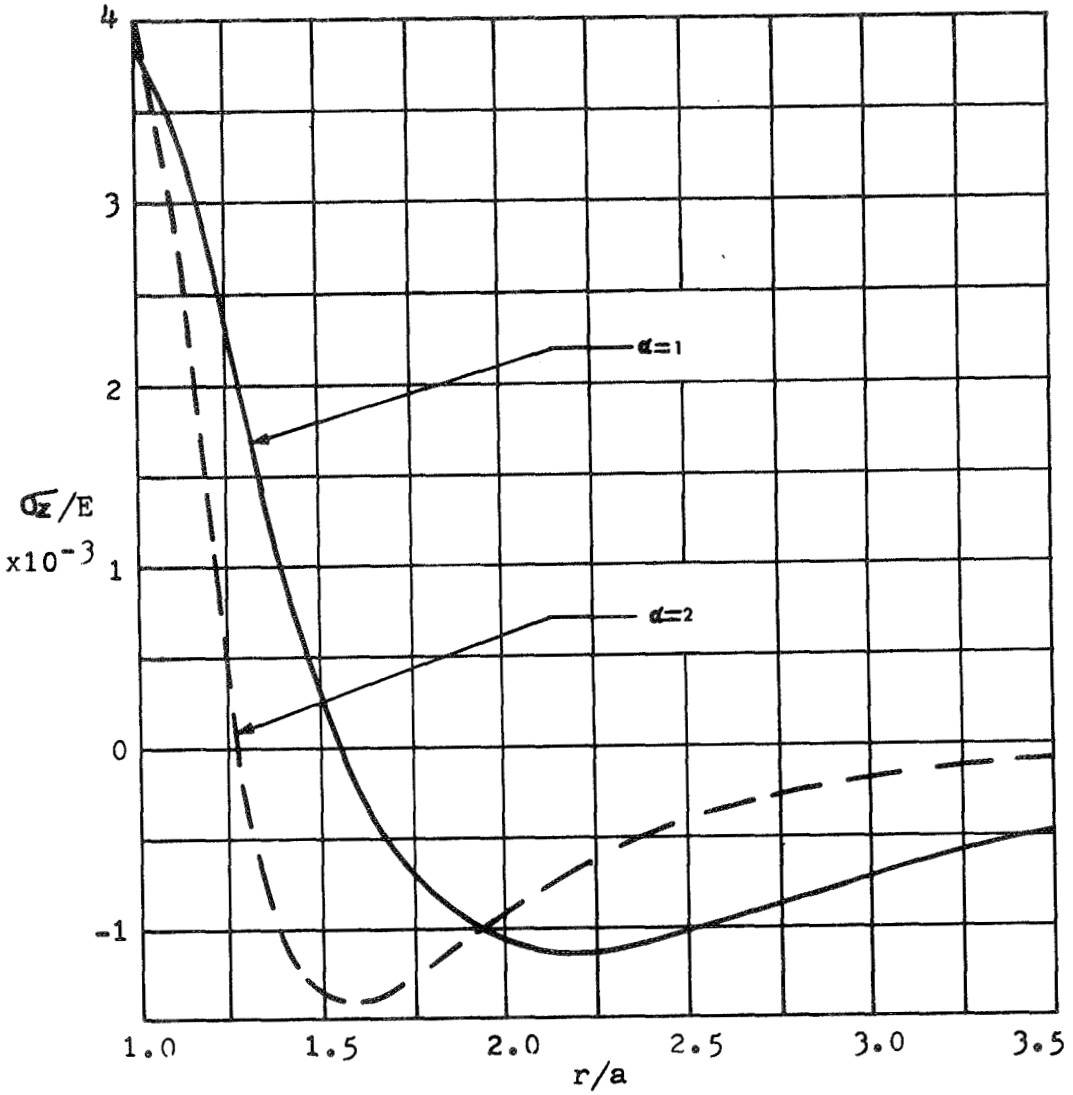

Figure 11. Nondimensional longitudinal stress as a function of radial coordinate.

$\zeta = .5 \qquad \beta = .01 \qquad \phi = .020833$

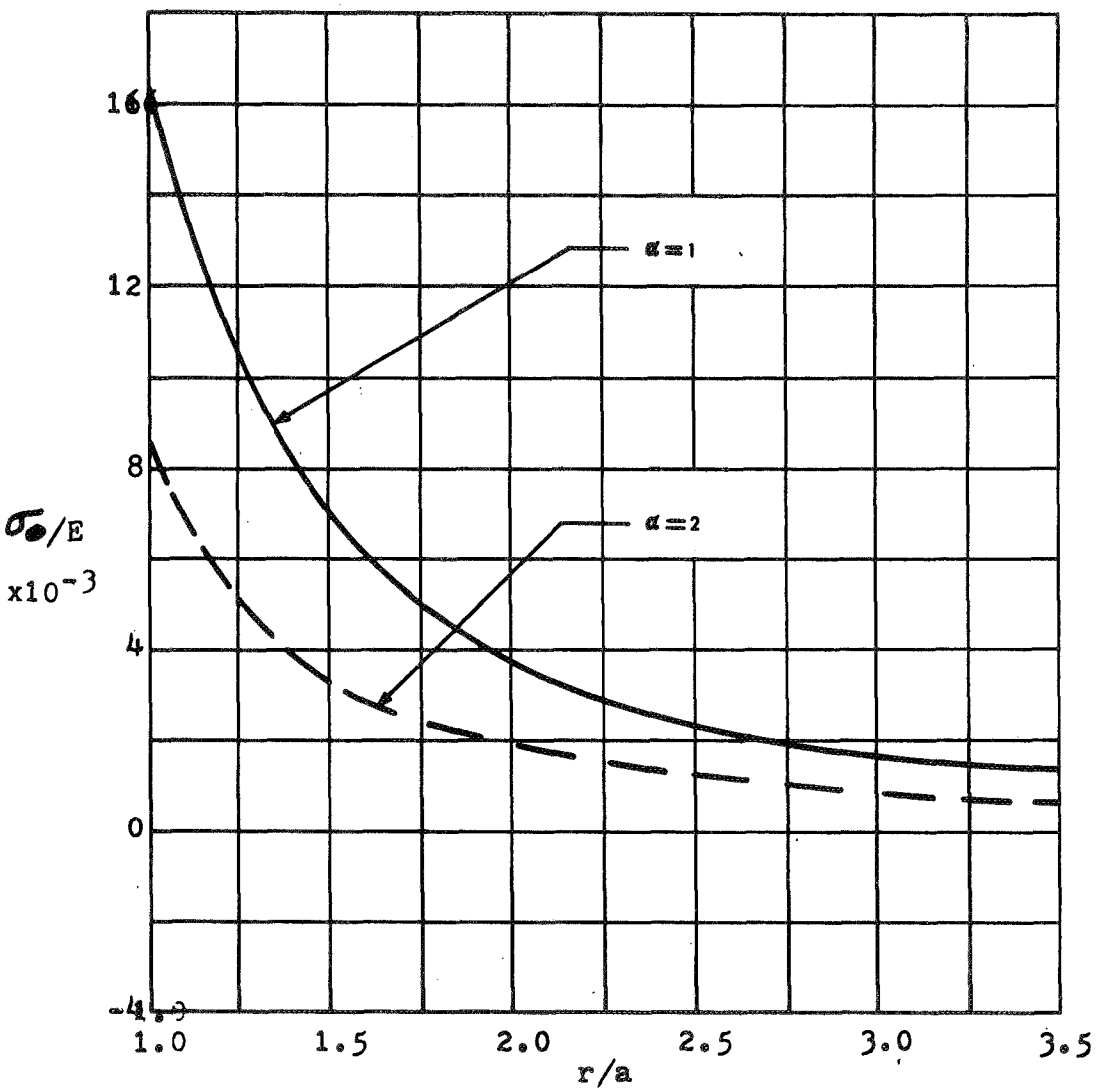

Figure 12. Nondimensional circumferential stress as a function of radial coordinate.

$\zeta = .5 \quad \beta = .01 \quad \phi = .020833$

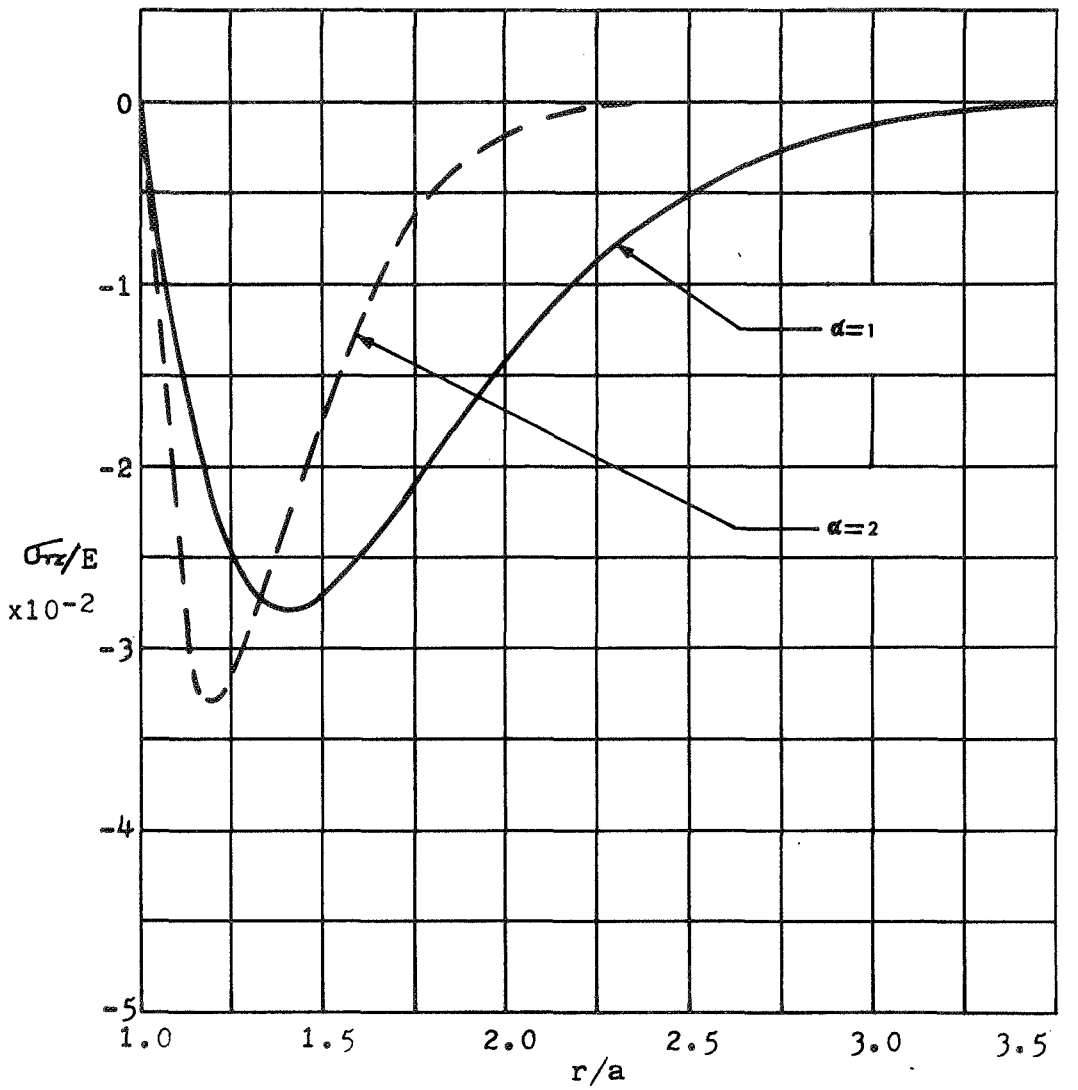

Figure 13. Nondimensional shear stress as a function of radial coordinate.

$\zeta = .5 \quad \beta = .01 \quad \phi = .020833$

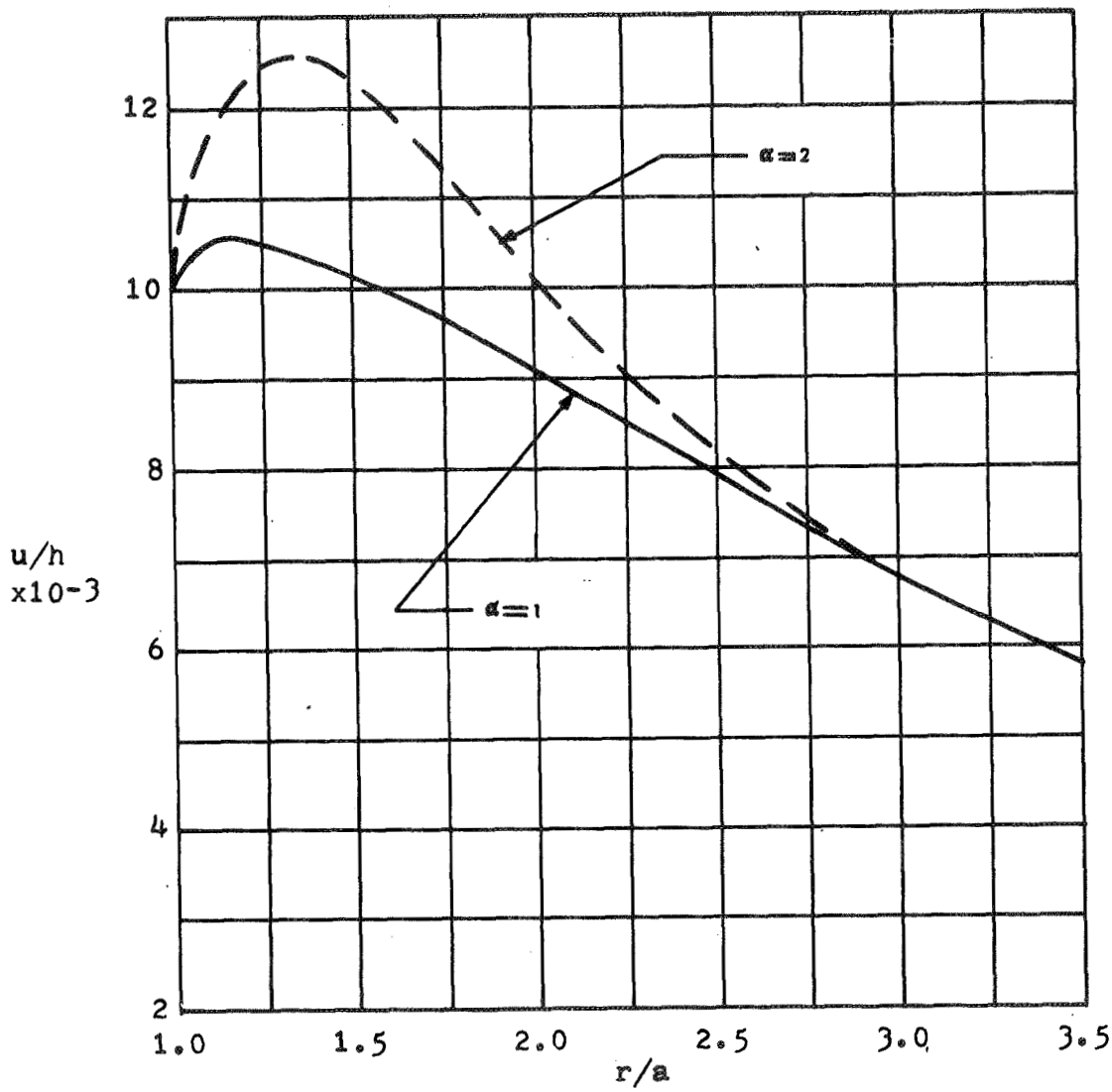

Figure 14. Nondimensional radial displacement as a function of radial coordinate.

$\zeta = 1.0 \quad \beta = .01 \quad \Phi = .020833$

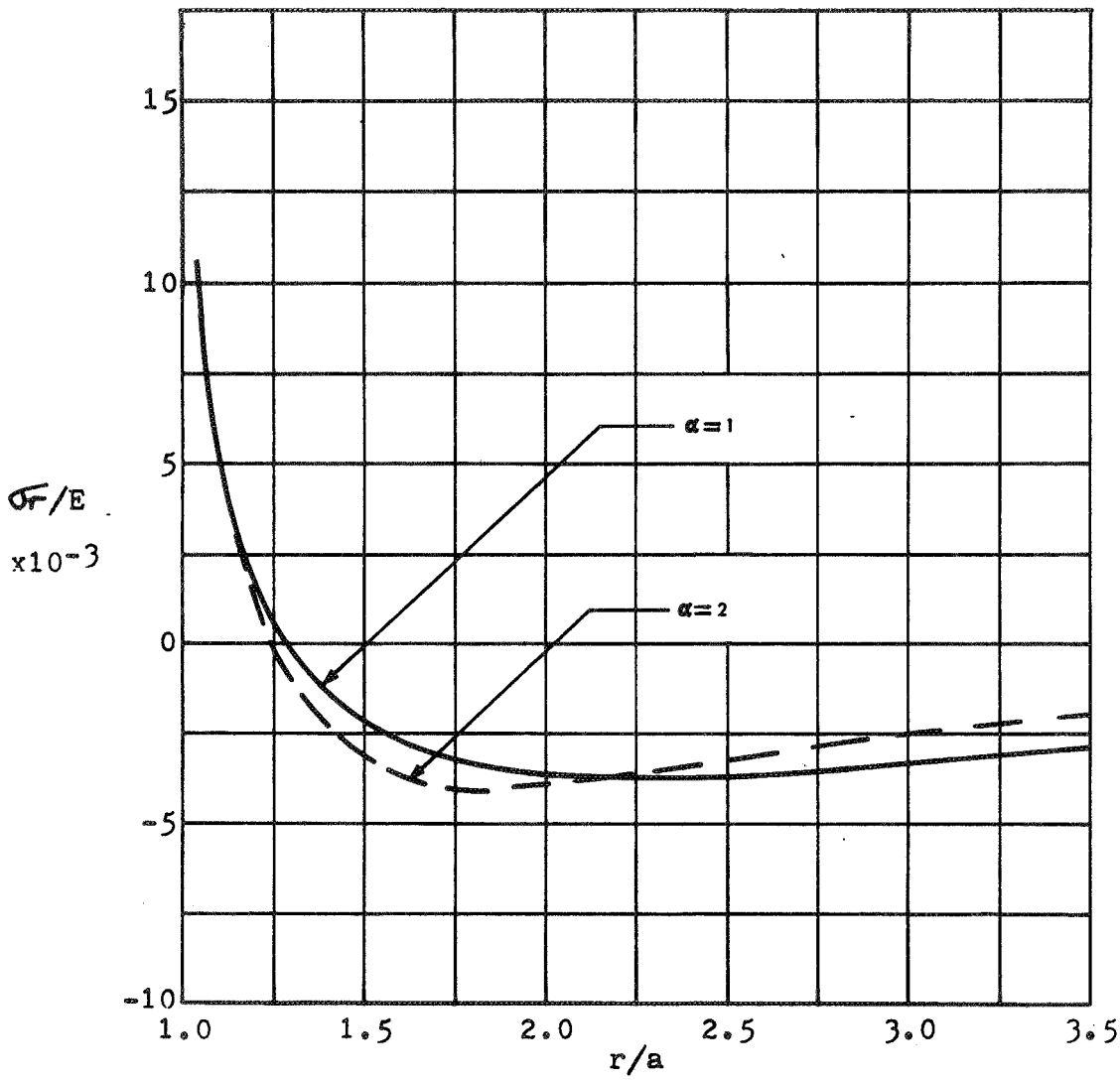

Figure 15. Nondimensional radial stress as a function of radial coordinate.

$\zeta = 1.0 \quad \beta = .01 \quad \phi = .020833$

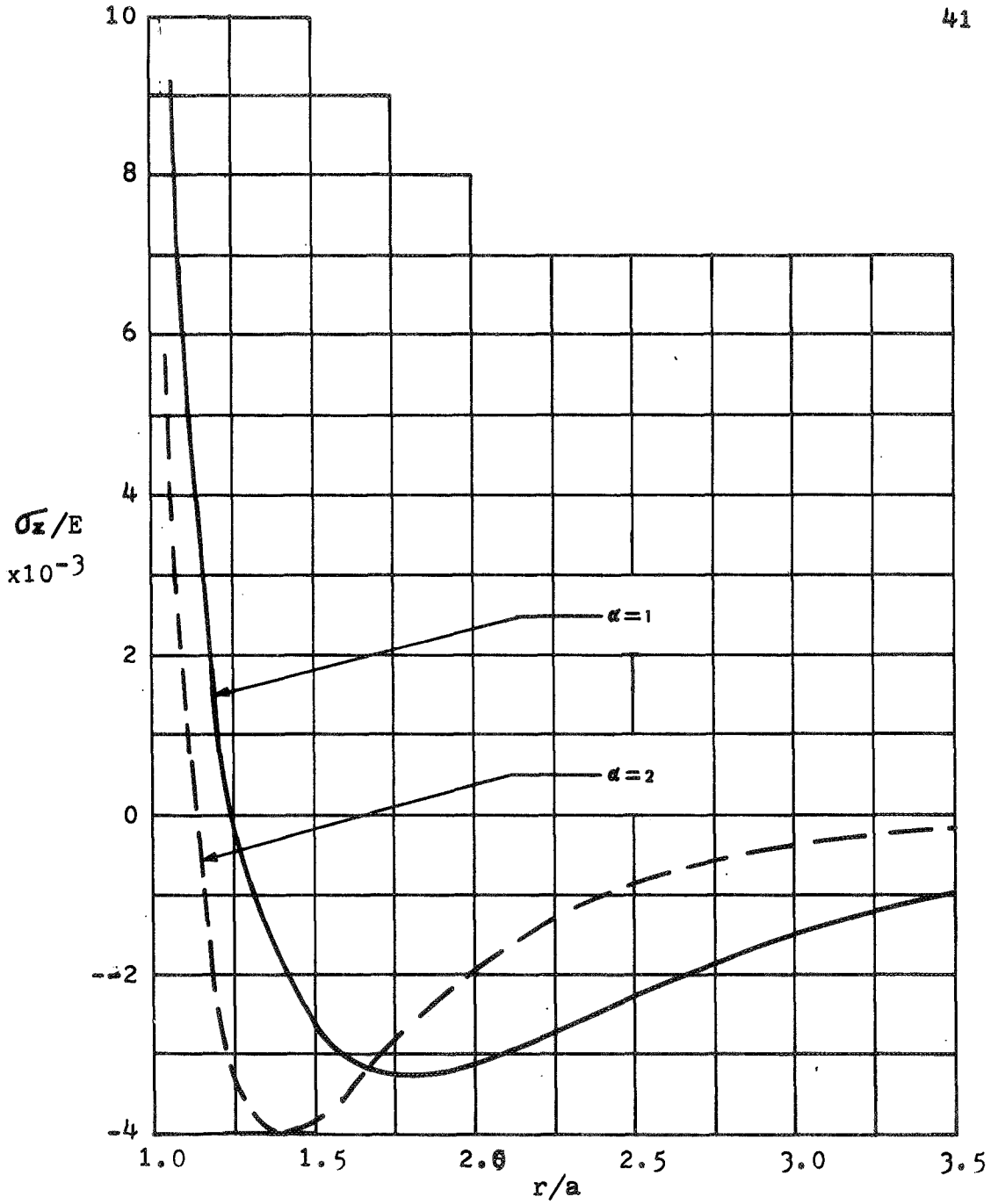

Figure 16. Nondimensional longitudinal stress as a function of radial coordinate.

$\zeta = 1.0 \quad \beta = .01 \quad \phi = .020833$

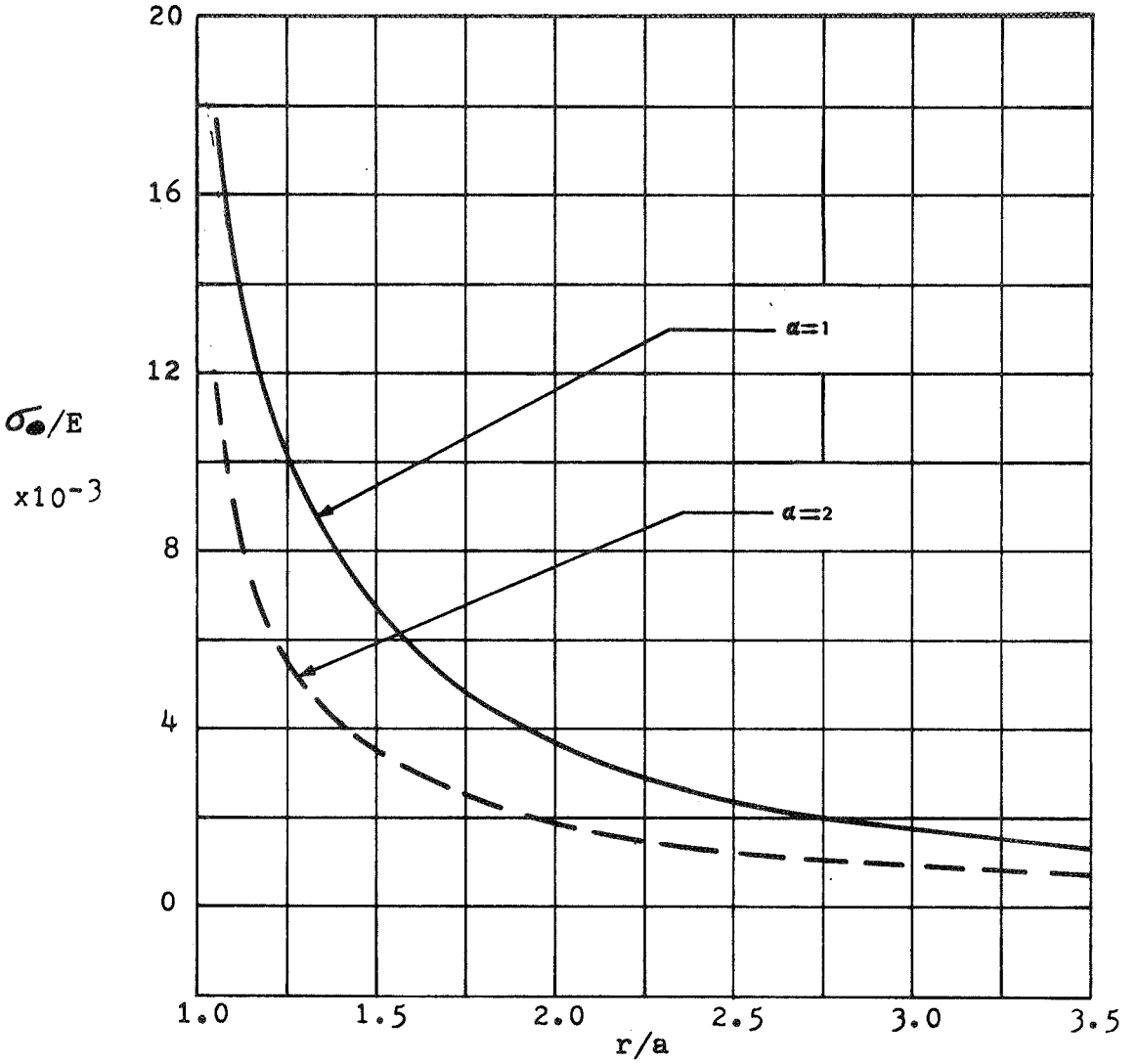

Figure 17. Nondimensional circumferential stress as a function of radial coordinate.

$\zeta = 1.0 \quad \beta = .01 \quad \phi = .020833$

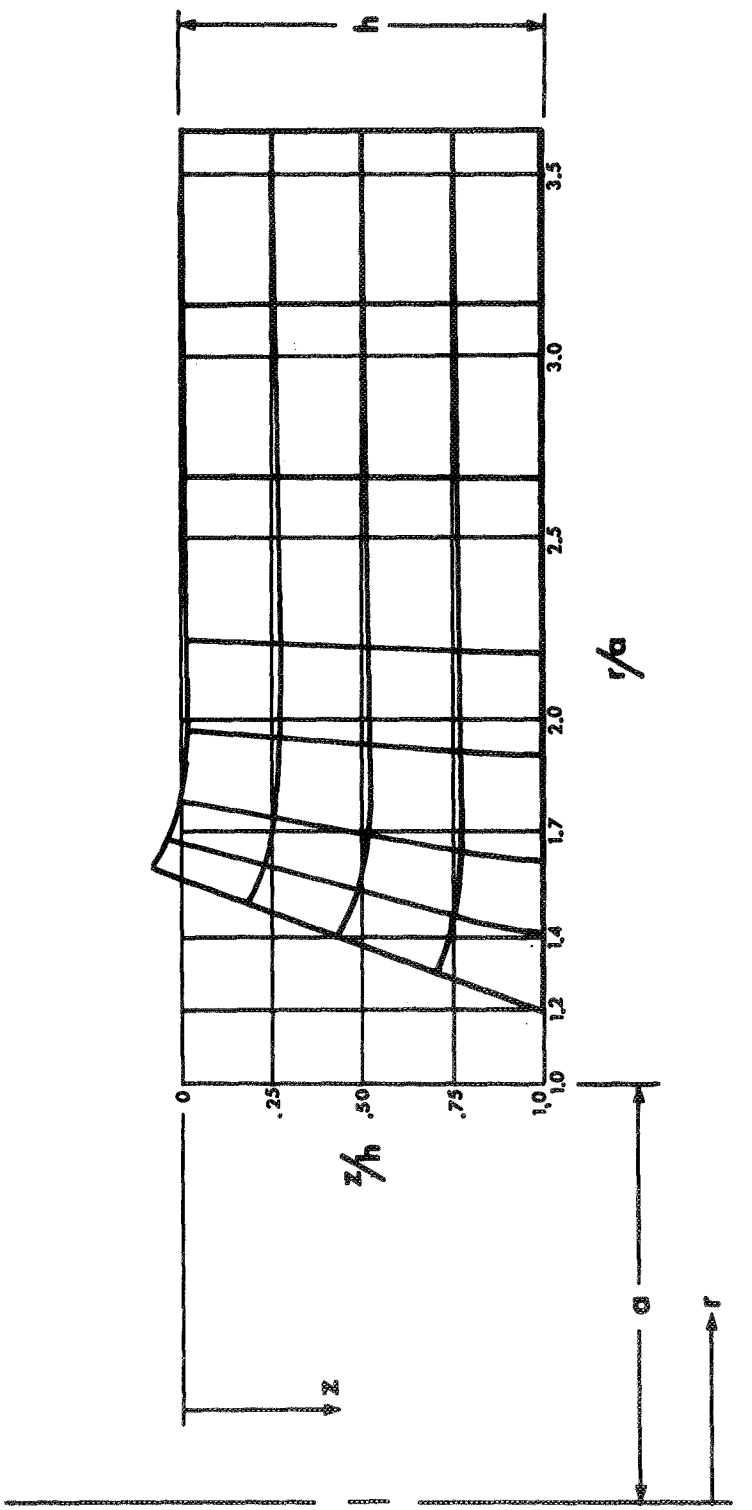

Figure 18. Deformation pattern, $\alpha = 1.0$.

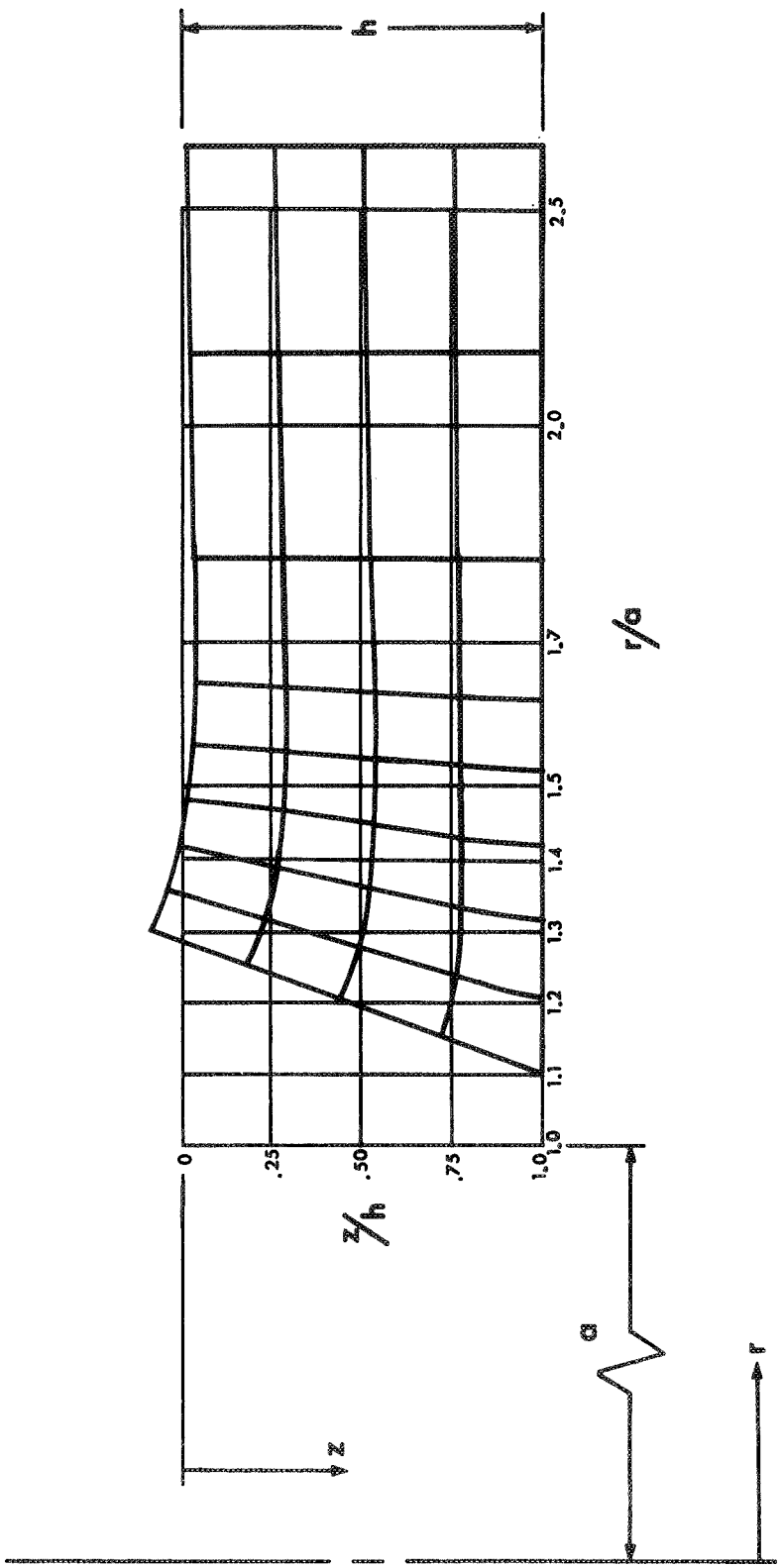

Figure 19. Deformation pattern, $\alpha = 2.0$.

CHAPTER V

SUMMARY AND CONCLUSIONS

The problem of an elastic layer with a transverse cylindrical hole being subjected to an axially-symmetric radial deformation was investigated. The solution to this problem was achieved by use of extended Hankel transforms. The solution was based on transforming Navier's equations of elasticity in the radial coordinate r and solving the resulting ordinary differential equations in the axial coordinate z. The solution of these differential equations provided the displacement functions. The stresses were obtained by use of stress-strain relations. Inversion of the displacement and stress functions required the numerical evaluation of infinite integrals.

With the exception of the singularity, the curves for stresses and displacements were seen to behave in a very normal manner. The imposed radial displacement on the cylindrical boundary is obviously impractical. One could not expect to maintain the sharp corner and remain within the confines of linear elasticity. The practical implication of this singularity (and the tensile radial stress) can be understood by considering a large disk of thickness $2k$ with a transverse cylindrical hole of radius a. Consider this disk to be

shrink-fitted (frictionless) onto a shaft with a circumferential V-groove having the geometry shown in Fig. 3. It can be deduced from the results of this study that the zone of tensile radial stress would not be in contact with the shaft. Instead, the cylindrical surface of the disk would maintain a smooth shape in keeping with the boundary conditions of zero shear stress. At $z = \ell$, the cylindrical surface would be perpendicular to the radial axis.

It is further concluded that, while the forward transformations of Navier's equations and the analytical solutions thereof are relatively straightforward, the inversion process requires special attention. It is felt the technique presented herein is an acceptable method for numerically evaluating the infinite inversion integrals.

REFERENCES

1. Scott, R.A., and Miklowitz, J., "Transient Compressional Waves in an Infinite Elastic Plate With a Circular Cylindrical Cavity," J. Applied Mechanics, Vol. 31, (1964), pp. 627-634.

2. Seco, J.J., "Use of Generalized Hankel Transforms in Solution of Some Axially-Symmetric Problems in Heat Conduction," University of Houston Thesis, 1969.

3. Weber, H., Verber eine Darstellung Will Kurlicher Functionen durch Bellel'sche Functionen, Math. Annelen, Vol. 6, (1873), p. 154.

4. Orr, W.M., "Extensions of Fourier's and the Bessel-Fourier Theorems," Proc. Royal Irish Acad., Vol. 27, (1909), p. 222.

5. Titchmarsh, E.C., "Weber's Integral Theorem," Proc. London Math. Soc., Vol. 22, (1923), pp. 15-24.

6. Titchmarsh, E.C., Eigenfunction Expansion, Part I, Second Edition, Oxford University Press, London, 1962.

7. Olesiak, Z., "Annular Punch on Elastic Semi-Space," Archiwum Mechaniki Stosowanej (in English), Vol. 4, (1965), p. 634.

8. Sneddon, I.N., Fourier Transforms, McGraw-Hill Book Co., Inc., New York, 1951, p. 452.

9. Churchill, R.V., Operational Mathematics, McGraw-Hill Book Co., Inc., New York, 1958, pp. 30-35.

10. Timoshenko, S., and Goodier, J.N., Theory of Elasticity, McGraw-Hill Book Co., Inc., 1951, p. 59.

11. Longman, I.M., "Note on a Method for Computing Infinite Integrals of Oscillatory Functions," Cambridge Phil. Soc., Proc., Vol. 52, (1956), pp. 764-768.

12. Bromwich, T.J.I'a, Introduction to the Theory of Infinite Series, MacMillan & Co., Ltd., London, 1965, pp. 62-66.

13. Parlas, S., "Axisymmetric Contact of a Rigid, Bolt-Shaped Punch on the Elastic Half-Space With a Transverse, Circular Cylindrical Hole," Thesis (forthcoming), University of Houston, December, 1970.

14. Tranter, C.J., Bessel Functions With Some Physical Applications, Hart Publishing Co., Inc., New York, 1968, pp. 60-62.

15. Abramowitz, M. and Stegun, I.A., Handbook of Mathematical Functions, Dover Publications, Inc., New York, 1956, p. 364.

16. Gray, A., and Mathews, G.B., A Treatise on Bessel Functions, Dover Publications Inc., New York, 1966, p. 261.

APPENDICES

APPENDIX A

PROPERTIES OF THE TRANSFORM

The following properties of extended Hankel transforms are taken from Scott and Miklowitz [1]:

$$\int_a^\infty r \frac{df}{dr} R_1(s,r;a)\,dr = \left[r f R_1(s,r;a) \right]_a^\infty - s\bar{f}_0(s) \tag{A1}$$

$$\int_0^\infty r\left[\frac{d^2f}{dr^2} + \frac{1}{r}\frac{df}{dr} - \frac{f}{r^2}\right] R_1(s,r;a)\,dr =$$

$$= \left\{ \left[r\frac{df}{dr} + f \right] R_1(s,r;a) - sr f R_0(s,r;a) \right\}_a^\infty -$$

$$- s^2 \bar{f}_1(s) \tag{A2}$$

$$\int_a^\infty r\left[\frac{d^2f}{dr^2} + \frac{1}{r}\frac{df}{dr}\right] R_0(s,r;a)\,dr =$$

$$= \left[r\frac{df}{dr} R_0(s,r;a) + sr f R_1(s,r;a) \right]_a^\infty - s^2 \bar{f}_0(s) \tag{A3}$$

$$\int_0^\infty \frac{R_\nu(s,r;a)\,ds}{s\left[J_\nu^2(sa) + Y_\nu^2(sa) \right]} = -\frac{\pi a^\nu}{2 r^\nu} . \tag{A4}$$

Additional properties (see, for example, Reference 2) are:

$$R_0(s,a,a) = -\frac{2}{\pi s a} \tag{A5}$$

$$R_1(s,a,a) = 0 \tag{A6}$$

$$\frac{\partial}{\partial \tau}\left[R_0(s,\tau,a)\right] = -s R_1(s,\tau,a) \tag{A7}$$

$$\frac{\partial}{\partial \tau}\left[\tau R_0(s,\tau,a)\right] = R_0(s,\tau,a) - s\tau R_1(s,\tau,a) \tag{A8}$$

$$\frac{\partial}{\partial \tau}\left[R_1(s,\tau,a)\right] = s R_0(s,\tau,a) - \frac{1}{\tau} R_1(s,\tau,a) \tag{A9}$$

$$\frac{\partial}{\partial \tau}\left[\tau R_1(s,\tau,a)\right] = s\tau R_0(s,\tau,a) . \tag{A10}$$

Parlas [13] showed by contour integration that the following condition is true:

$$\int_0^\infty \frac{R_0(s,\tau,a)\, ds}{J_1^2(as) + Y_1^2(as)} = 0 \qquad \tau > a . \tag{A11}$$

APPENDIX B

ROOTS OF THE INTEGRANDS IN THE INVERSE TRANSFORMS

In order to find the roots of the inverse integrands,

$$\frac{s\,\bar{F}_0(x)\,R_0(s;\tau;a)\,ds}{J_1^2(as)+Y_1^2(as)} \tag{B1}$$

$$\frac{s\,\bar{F}_1(x)\,R_1(s;\tau;a)\,ds}{J_1^2(as)+Y_1^2(as)}\,, \tag{B2}$$

it is only necessary to determine the roots of $R_0(s;\tau;a)$ and $R_1(s;\tau;a)$ which are defined as follows:

$$R_0(s;\tau;a) = J_0(s\tau)\,Y_1(sa) - J_1(sa)\,Y_0(s\tau) \tag{B3}$$

$$R_1(s;\tau;a) = J_1(s\tau)\,Y_1(sa) - J_1(sa)\,Y_1(s\tau)\,. \tag{B4}$$

The derivation of the expressions for the roots utilizes Stoke's method (see, for example, Reference 14). The following are asymtotic approximations for Bessel functions of the first and the second kind [15]:

$$J_\nu(x) \cong \sqrt{\frac{2}{\pi x}}\left[P(\nu,x)\cos\psi - Q(\nu,x)\sin\psi\right] \tag{B5}$$

$$Y_\nu(x) \cong \sqrt{\frac{2}{\pi x}}\left[P(\nu,x)\sin\psi + Q(\nu,x)\cos\psi\right]\,, \tag{B6}$$

where

$$P(\tau,x) = 1 - \frac{(4\tau^2-1)(4\tau^2-9)}{2!\,(8x)^2} + \frac{(4\tau^2-1)(4\tau^2-9)(4\tau^2-25)(4\tau^2-49)}{4!\,(8x)^4} \quad (B7)$$

$$Q(\tau,x) = \frac{4\tau^2-1}{8x} - \frac{(4\tau^2-1)(4\tau^2-9)(4\tau^2-25)}{3!\,(8x)^3} \quad (B8)$$

$$\chi = x - \left(\tfrac{3}{2}+\tfrac{1}{4}\right)\pi \,. \quad (B9)$$

Roots of $R_0(x,\tau a)$.

Given Eq. (B3) and letting $\rho_0 = sa$ and $\gamma = \tau/a$, Eq. (B3) becomes:

$$R_0(\rho_0,\gamma) = J_0(\gamma\rho_0)\,Y_1(\rho_0) - J_1(\rho_0)\,Y_0(\gamma\rho_0) \,. \quad (B10)$$

It follows that Eqs. (B5),(B6),(B7),(B8) and (B9) can be written:

$$J_0(\gamma\rho_0) \cong \sqrt{\frac{2}{\pi\gamma\rho_0}}\left\{P^2(0,\gamma\rho_0) + Q^2(0,\gamma\rho_0)\right\}^{1/2}\cos\left(\gamma\rho_0 - \tfrac{\pi}{4} - \omega_1\right) , \quad (B11)$$

where

$$\omega_1 = \tan^{-1}\left(\frac{1}{8\gamma\rho_0} - \frac{33}{(8\gamma\rho_0)^3}\right)$$

$$J_1(\rho_0) \cong \sqrt{\frac{2}{\pi\rho_0}}\left\{P^2(1,\gamma\rho_0) + Q^2(1,\gamma\rho_0)\right\}^{1/2}\cos\left(\rho_0 - \tfrac{3\pi}{4} - \omega_2\right) , \quad (B12)$$

where

$$\omega_2 = \tan^{-1}\left(-\frac{3}{8\rho_0} + \frac{75}{(8\rho_0)^3}\right)$$

$$Y_0(\gamma\rho_0) \cong \sqrt{\frac{2}{\pi\gamma\rho_0}}\left\{P^2(0,\gamma\rho_0)+Q^2(0,\gamma\rho_0)\right\}\sin\left(\rho_0\gamma-\tfrac{\pi}{4}+\omega_3\right), \quad \text{(B13)}$$

where $$\omega_3 = \tan^{-1}\left(-\frac{1}{8\gamma\rho_0}+\frac{33}{(8\gamma\rho_0)^3}\right)$$

$$Y_1(\rho_0) \cong \sqrt{\frac{2}{\pi\rho_0}}\left\{P^2(1,\rho_0)+Q^2(1,\rho_0)\right\}^{1/2}\sin\left(\rho_0-\tfrac{3\pi}{4}+\omega_4\right), \quad \text{(B14)}$$

where $$\omega_4 = \tan^{-1}\left(\frac{3}{8\rho_0}-\frac{75}{(8\rho_0)^3}\right).$$

Setting Eq. (B10) equal to zero and realizing the equalities that exist with the $\sqrt{\frac{2}{\pi x}}\left\{P^2(z,x)+Q^2(z,x)\right\}^{1/2}$ terms, the following simplification results:

$$\sin\left(\rho_0-\gamma\rho_0-\pi/2+\frac{3}{8\rho_0}-\frac{84}{512\rho_0^3}+\frac{1}{8\gamma\rho_0}-\right.$$

$$\left.-\frac{25}{384(\gamma\rho_0)^3}\right) = 0. \quad \text{(B15)}$$

For positive values of ρ_0, the zeros of Eq. (B15) are represented by:

$$\rho_0-\gamma\rho_0-\pi/2+\frac{3}{8\rho_0}-\frac{84}{512\rho_0^3}+\frac{1}{8\gamma\rho_0}-\frac{25}{384(\gamma\rho_0)^3} = -n\pi \quad \text{(B16)}$$

$$\text{FOR } n = 0, 1, 2, 3, \cdots.$$

Rearranging to solve for ρ_0 in terms of n gives:

$$\rho_0 = \frac{(n-1/2)\pi}{\gamma-1}+\frac{1}{8\rho_0(\gamma-1)}+\frac{3}{8\rho_0(\gamma-1)}-$$

$$-\frac{84}{512\rho_0^3(\gamma-1)}-\frac{25}{384(\gamma\rho_0)^3(\gamma-1)}, \quad \text{(B17)}$$

where ρ_0 represents the nth root of Eq. (B10).

Letting

$$\frac{(n-1/2)\pi}{\gamma-1} = \delta \tag{B18}$$

and assuming

$$\rho_0 = \delta + \frac{\delta_1}{\delta} + \frac{\delta_2}{\delta^3} + \cdots, \tag{B19}$$

it can be shown the expression for computing the nth root of $R_0(\rho,\gamma)$ is:

$$\rho_0(n,\gamma) = \frac{(n-1/2)\pi}{\gamma-1} + \frac{3\gamma+1}{8\gamma(n-1/2)\pi} - \frac{63\gamma^5 - 72\gamma^4 + 45\gamma^3 - 5\gamma^2 - 56\gamma - 25}{512\gamma^3\pi^3(n-1/2)^3}. \tag{B20}$$

Roots of $R_1(s,\tau,a)$

Using the same procedure as before, the expression for computing the nth root of $R_1(\rho,\gamma)$ is:

$$\rho_1(n,\gamma) = \frac{n\pi}{\gamma-1} + \frac{3(\gamma-1)}{8\gamma(n\pi)} - \frac{21\gamma^5 - 24\gamma^4 - 33\gamma^3 + 33\gamma^2 + 24\gamma - 21}{128\gamma^3\pi^3 n^3}. \tag{B21}$$

Comment.

The expression for the roots of $R_1(s,\tau,a)$, Eq. (B21), is verified by Gray and Mathews [16]. Data generated from Eq. (B20) have been verified by the curves of the functions presented in Appendix C. There is slight error in the first root due to the asymtotic approximations of the the Bessel

functions being for large arguments. This error, however, had no effect on the results presented herein.

APPENDIX C

CURVES FOR INVERSION KERNELS AND SELECTED INTEGRANDS

Curves for the inversion kernels K_0 and K_1 and inversion integrands $\bar{u}K_1$ and $\bar{\sigma}_z K_0$ are presented as functions of the independent variable s. These curves are representative in nature and are not intended to imply specific importance.

The terms $\bar{u}$ and $\bar{\sigma}_z$ are defined in Chapter II of the text and K_0 and K_1 are defined as:

$$K_0 = \frac{s R_0(s,\alpha,\rho)}{J_1^2(\alpha s) + Y_1^2(\alpha s)} \tag{C1}$$

$$K_1 = \frac{s R_1(s,\alpha,\rho)}{J_1^2(\alpha s) + Y_1^2(\alpha s)} , \tag{C2}$$

where

$$R_0(s,\alpha,\rho) = J_0(\rho s) Y_1(\alpha s) - J_1(\alpha s) Y_0(\rho s) \tag{C4}$$

$$R_1(s,\alpha,\rho) = J_1(\rho s) Y_1(\alpha s) - J_1(\alpha s) Y_1(\rho s) . \tag{C5}$$

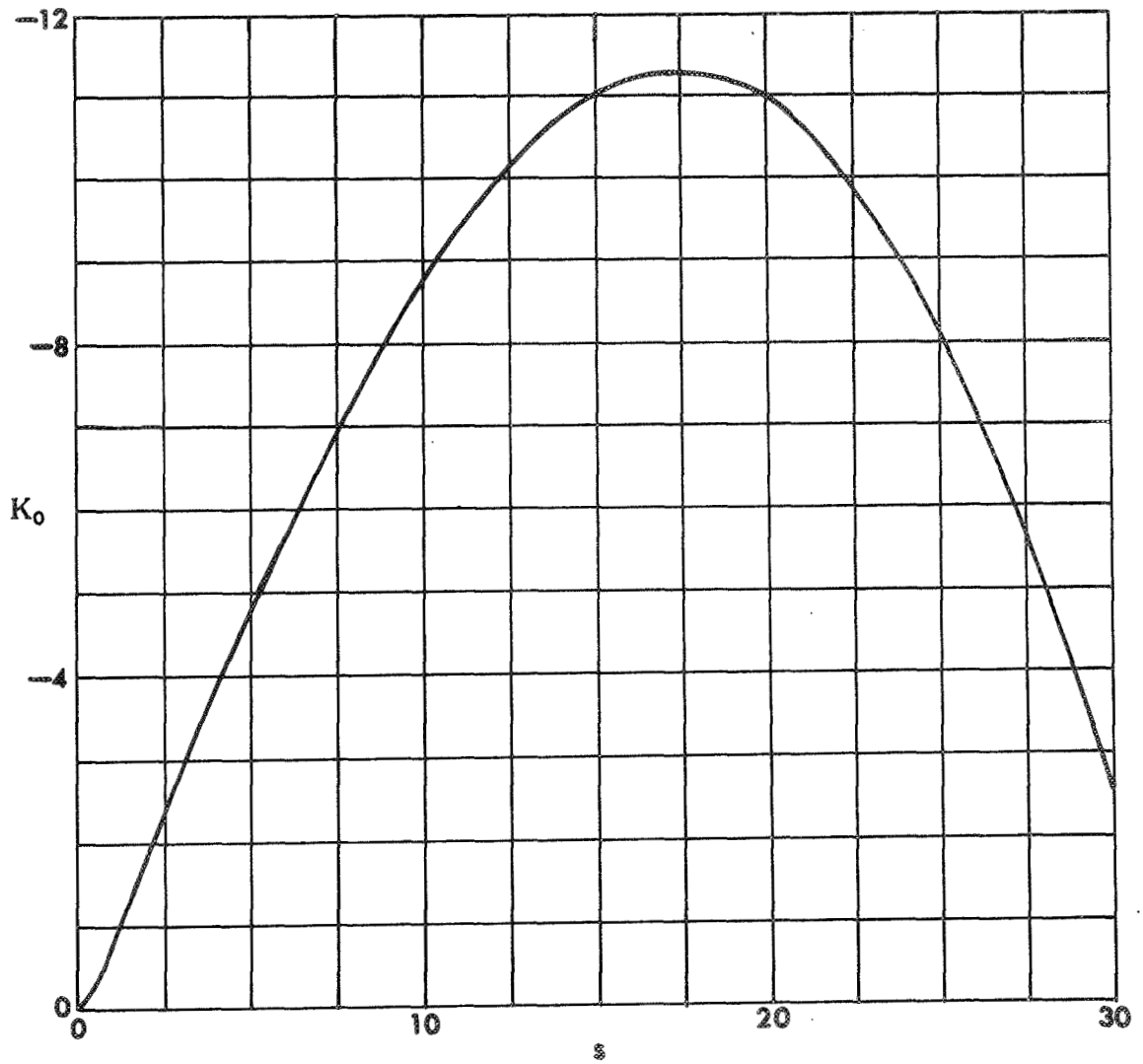

Figure C1. Zero-Order inversion kernel versus independent variable, r/a=1.05.

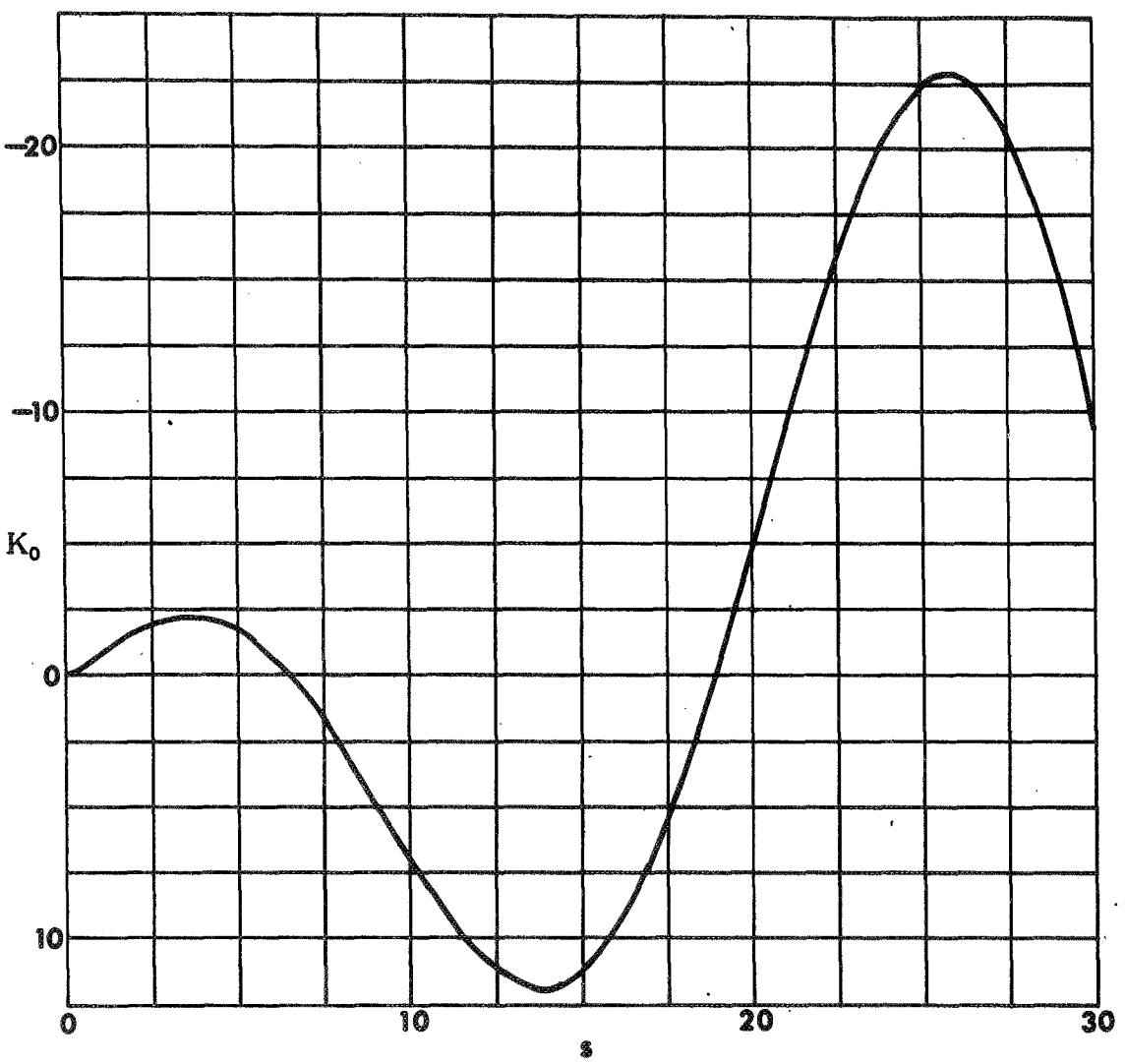

Figure C2. Zero-Order inversion kernel versus independent variable, r/a=1.25.

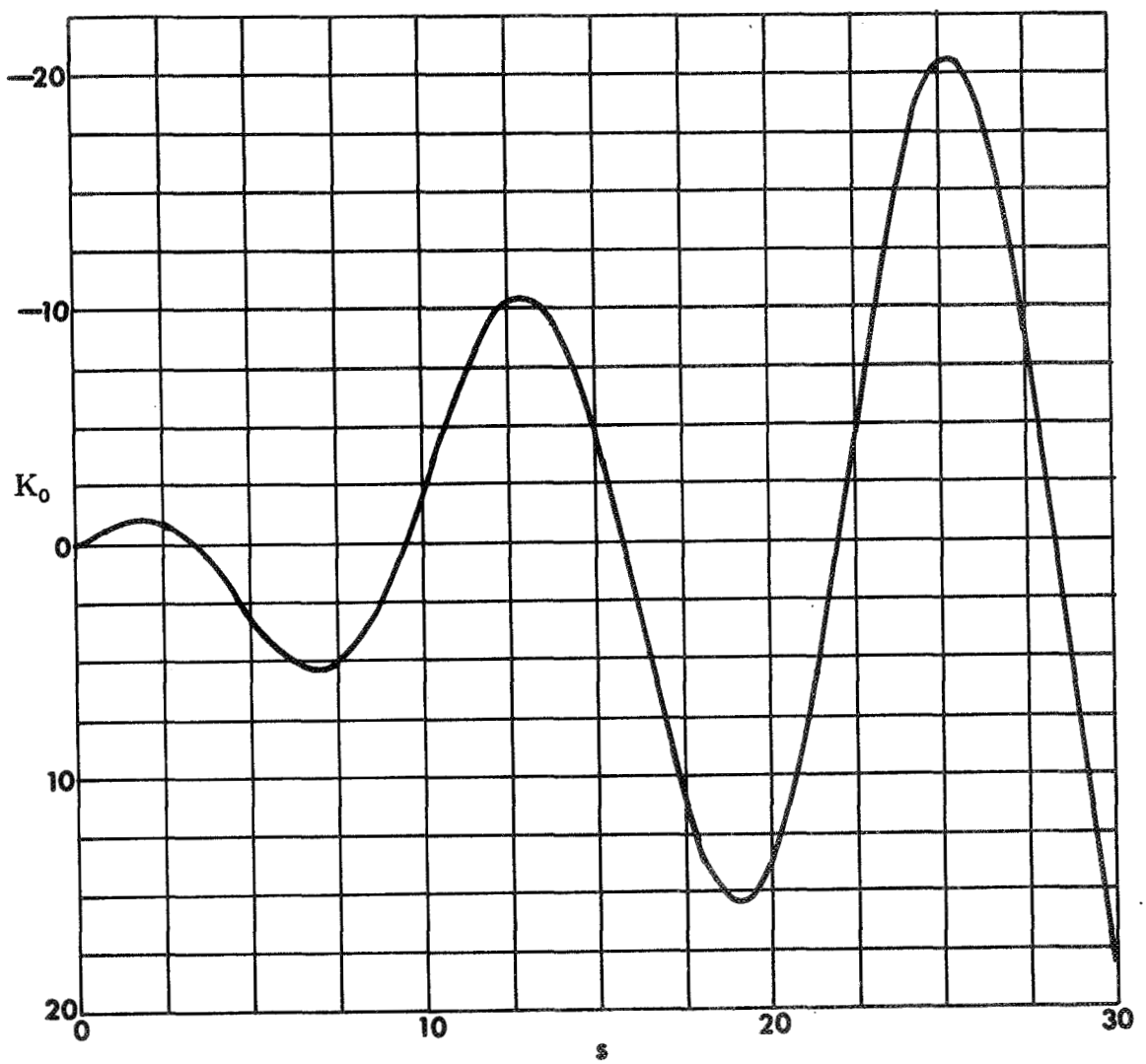

Figure C3. Zero-Order inversion kernel versus independent variable, r/a=1.5.

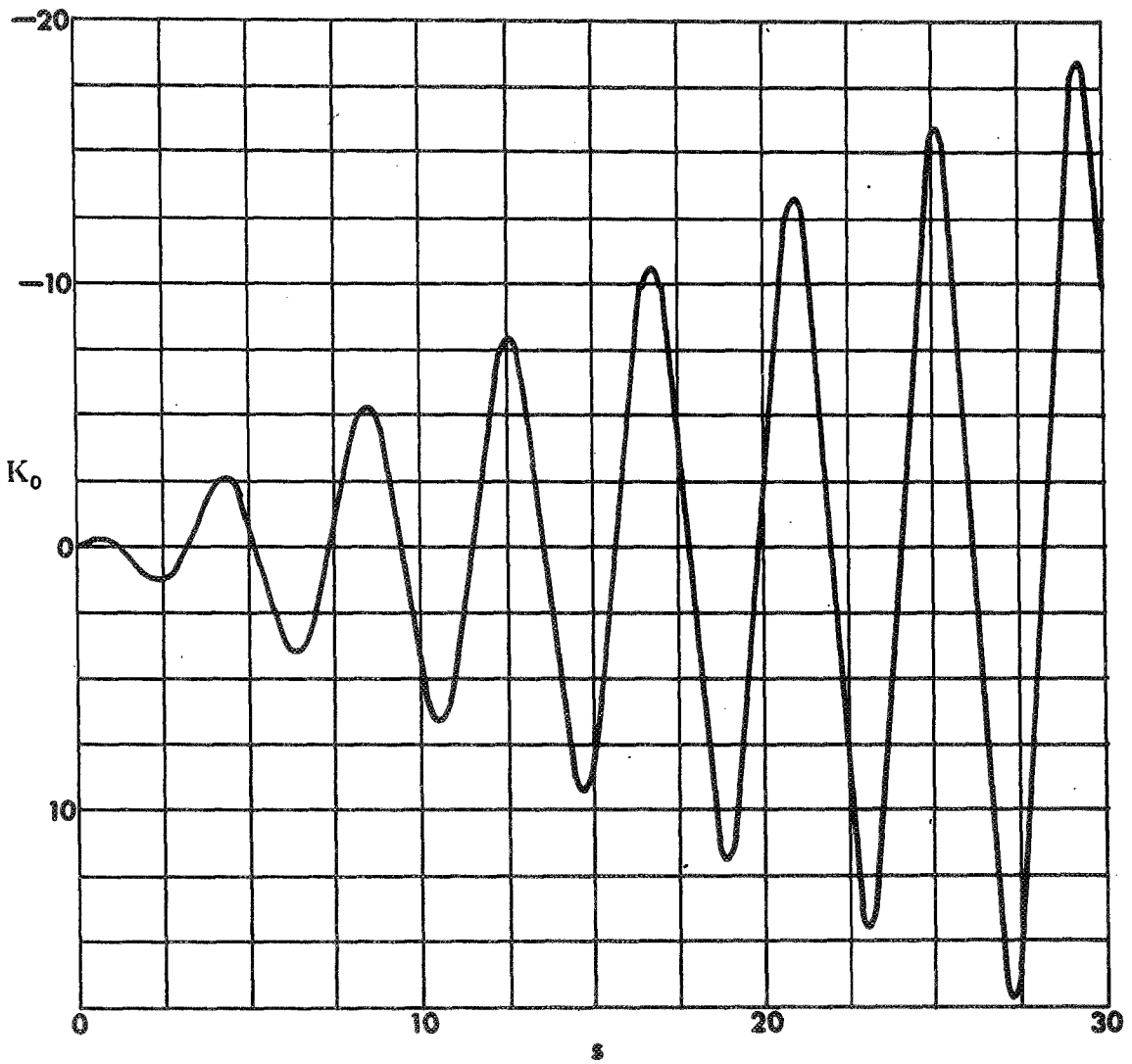

Figure C4. Zero-Order inversion kernel versus independent variable, r/a=2.5.

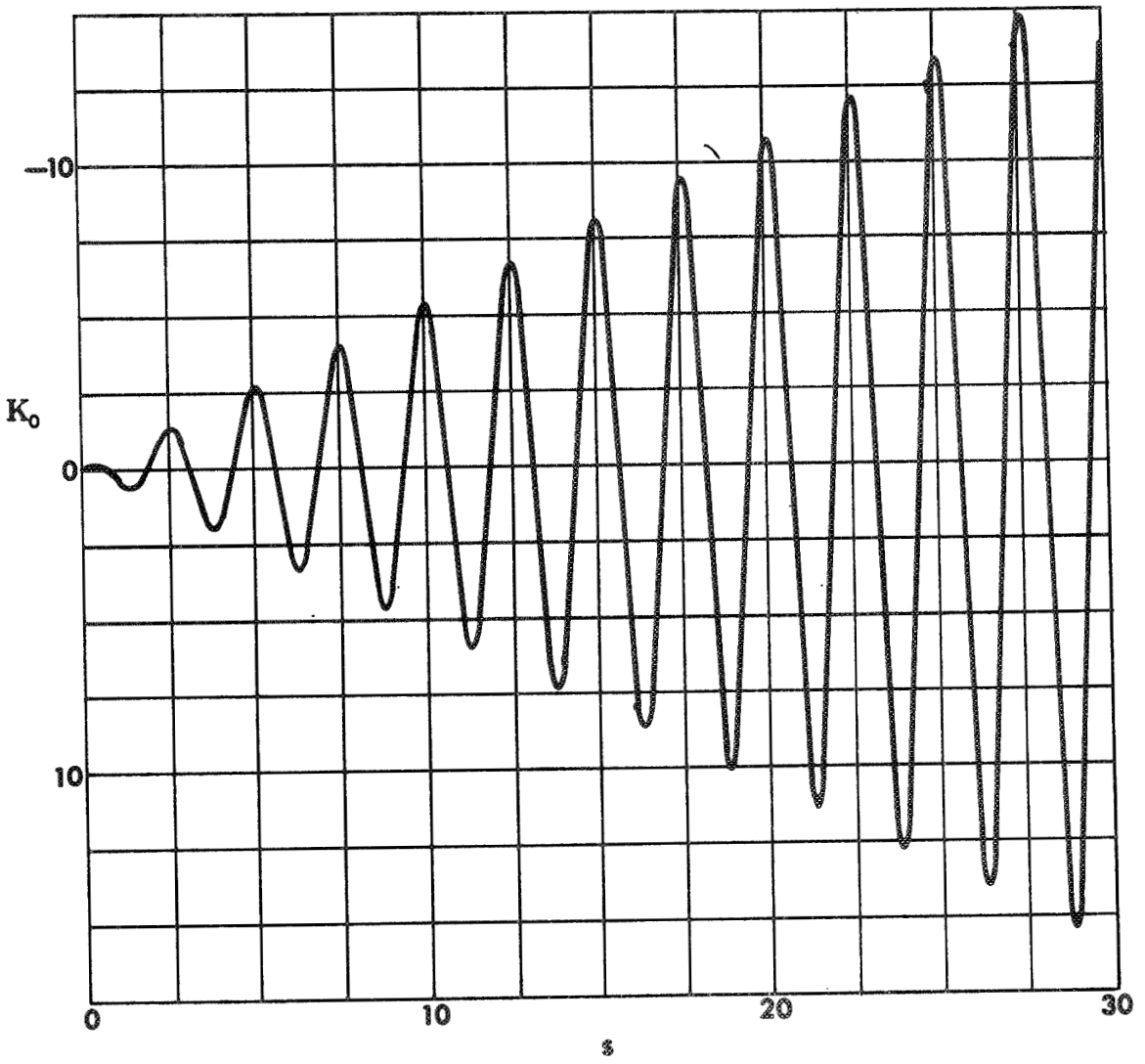

Figure C5. Zero-Order inversion kernel versus independent variable, r/a=3.5.

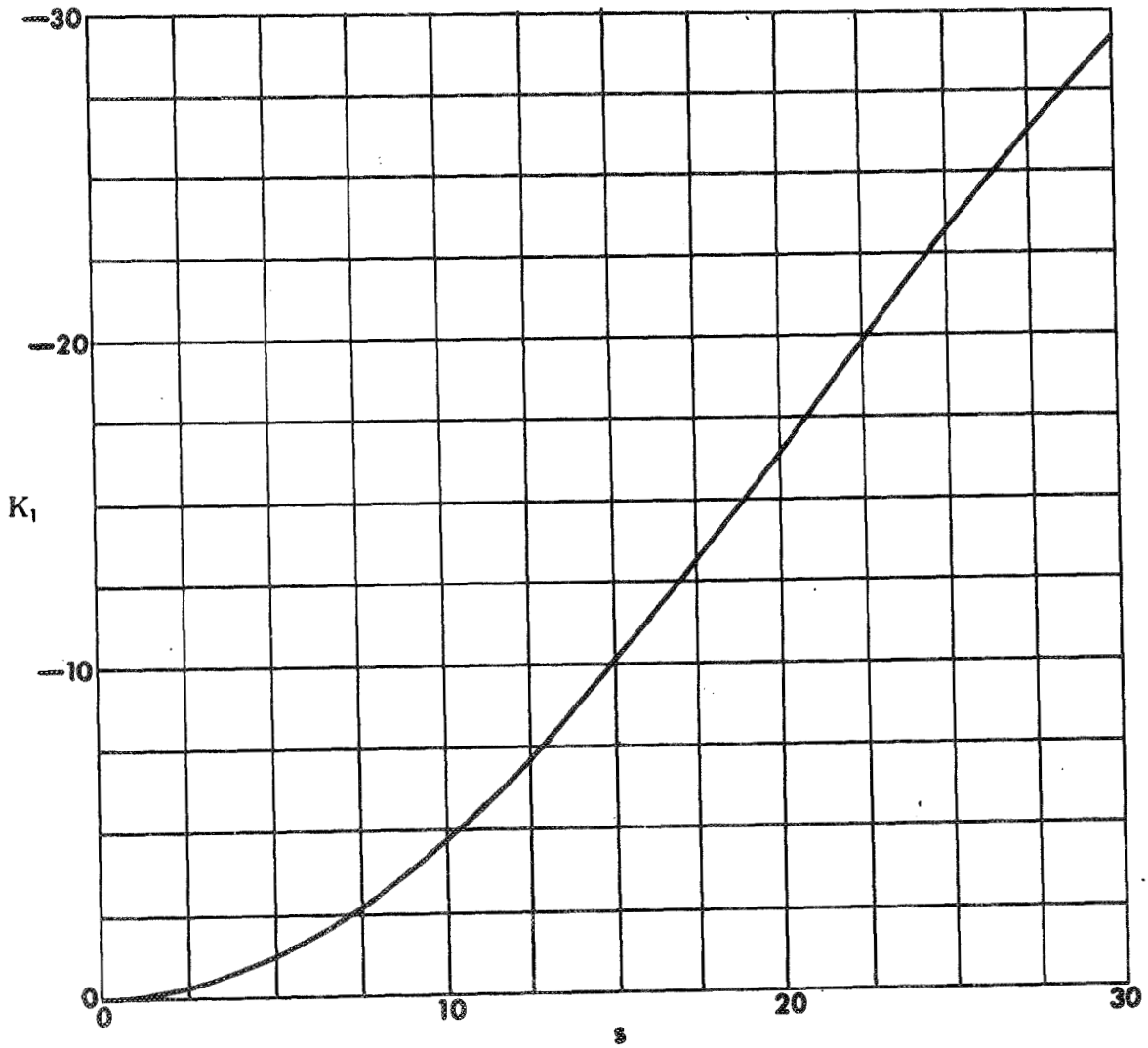

Figure C6. First-Order inversion kernel versus independent variable, r/a=1.05

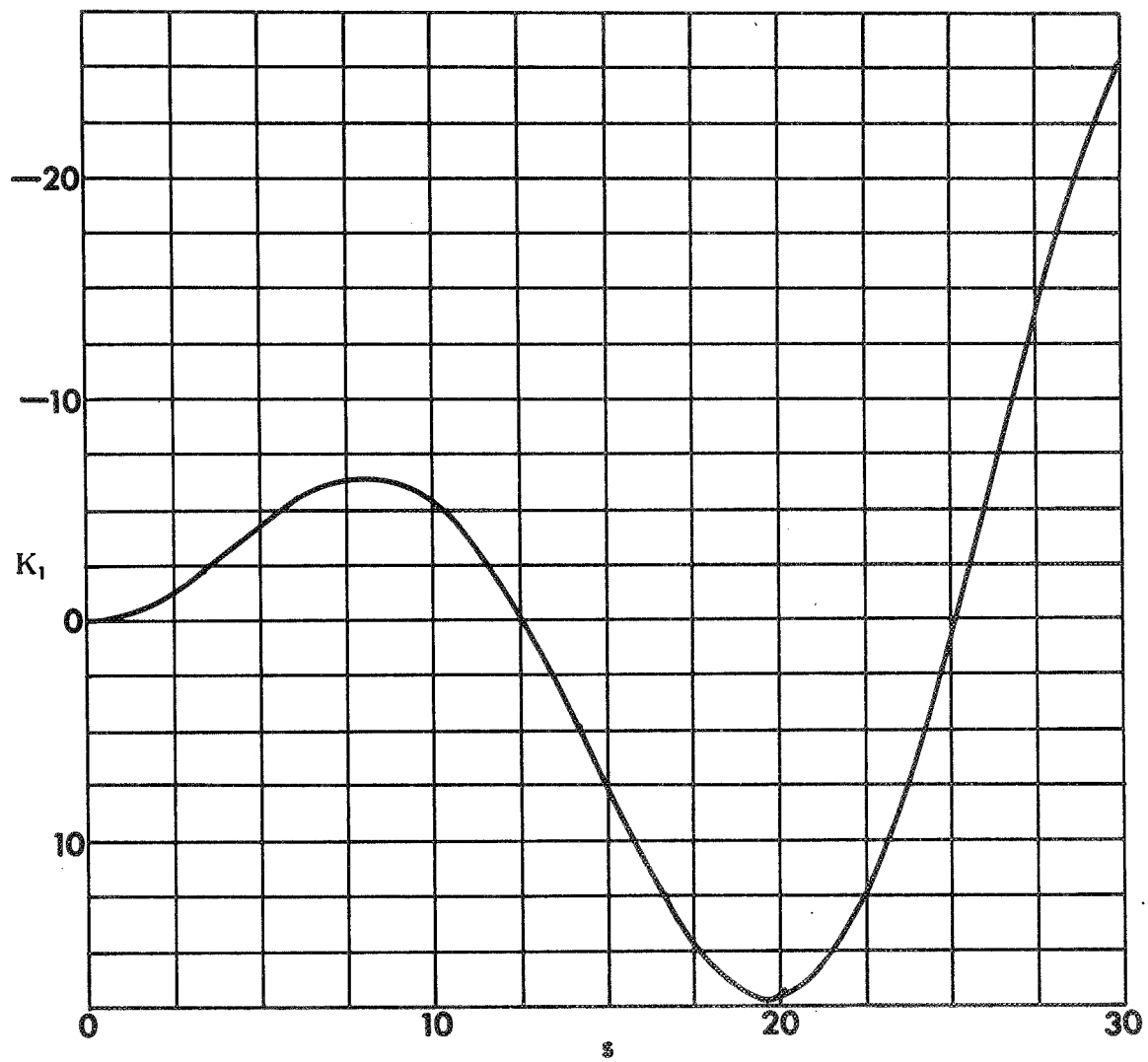

Figure C7. First-Order inversion kernel versus independent variable, r/a=1.25.

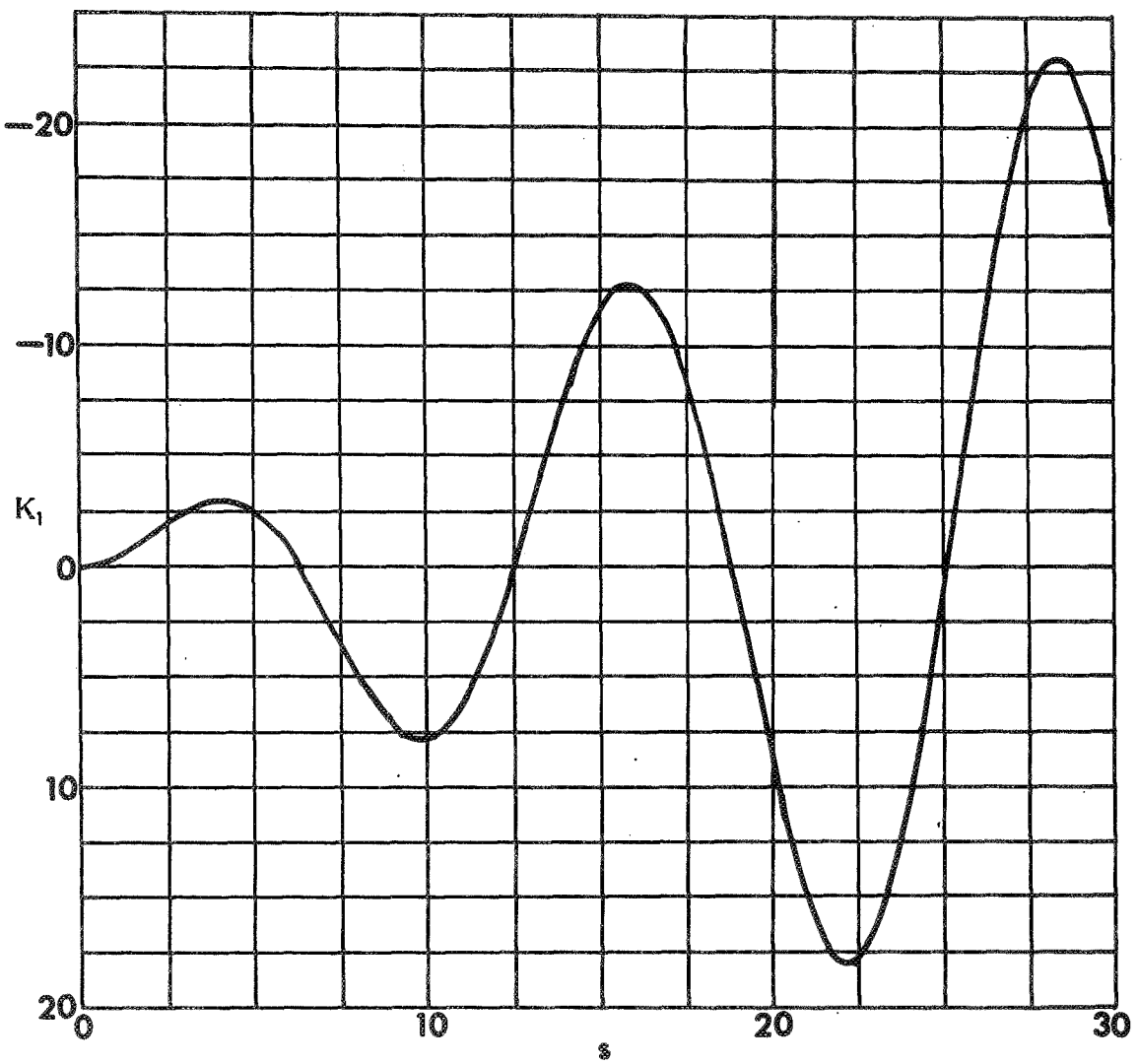

Figure C8. First-Order inversion kernel versus independent variable, r/a=1.5.

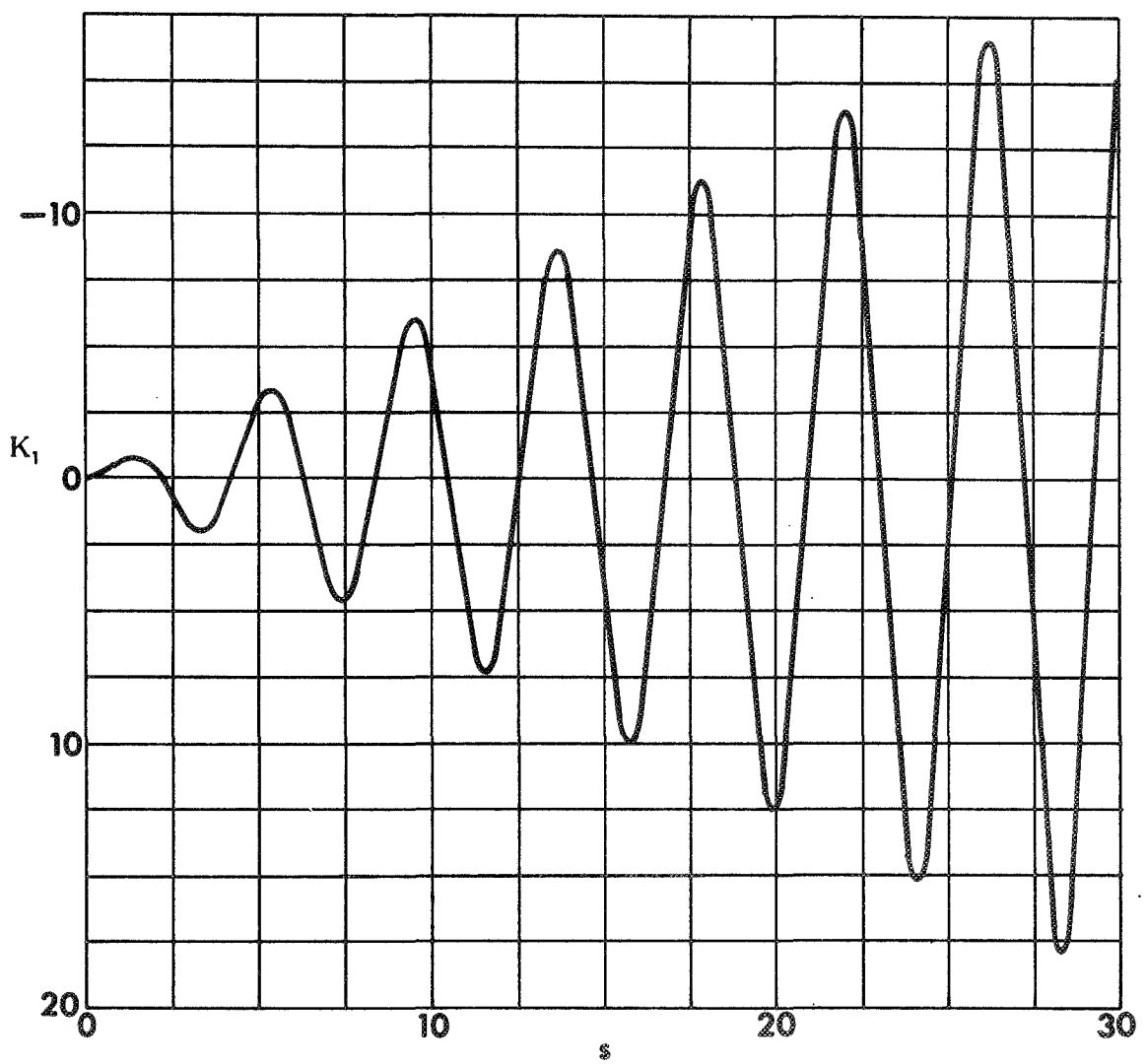

Figure C9. First-Order inversion kernel versus independent variable, r/a=2.5.

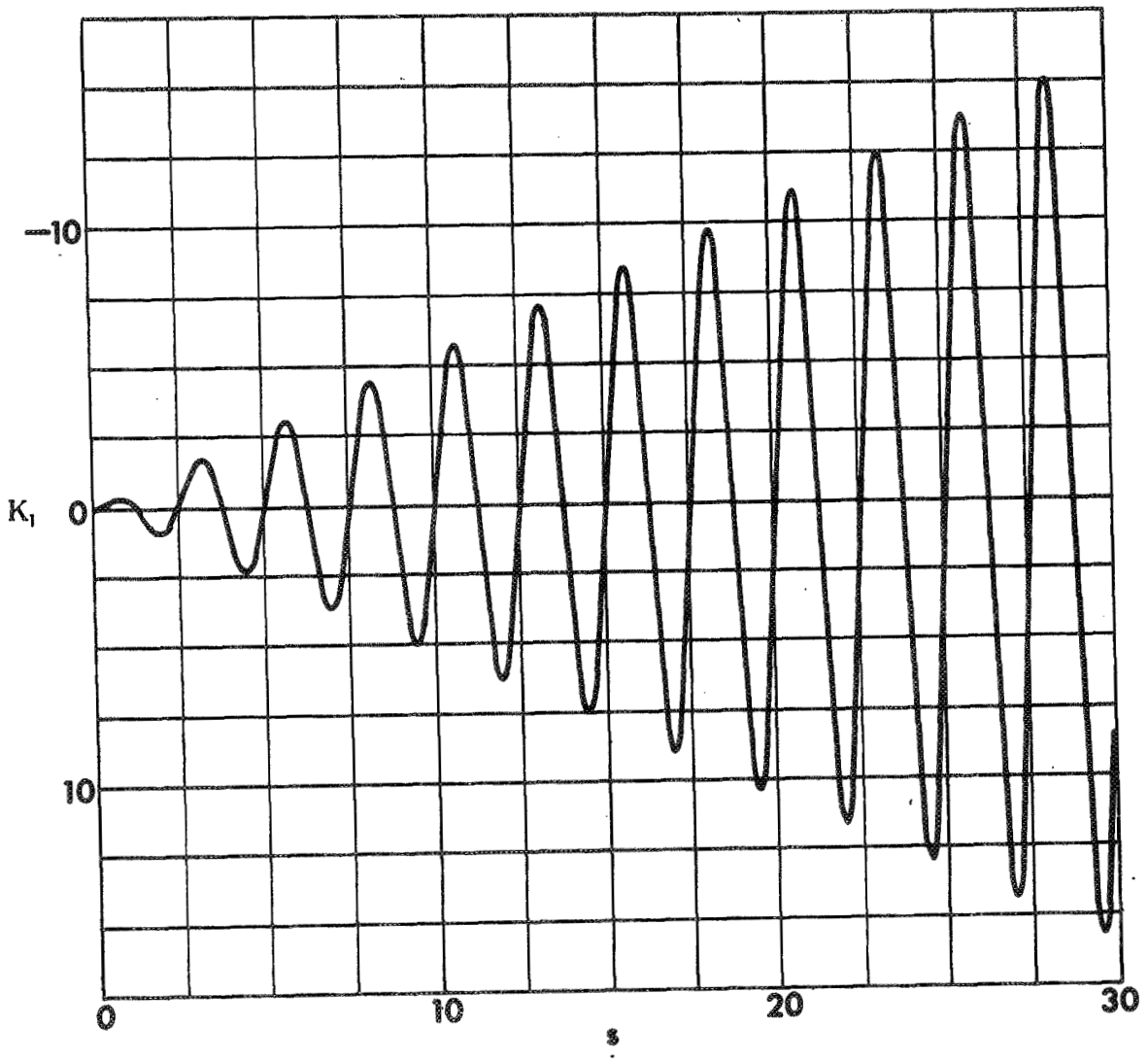

Figure C10. First-Order inversion kernel versus independent variable, r/a=3.5.

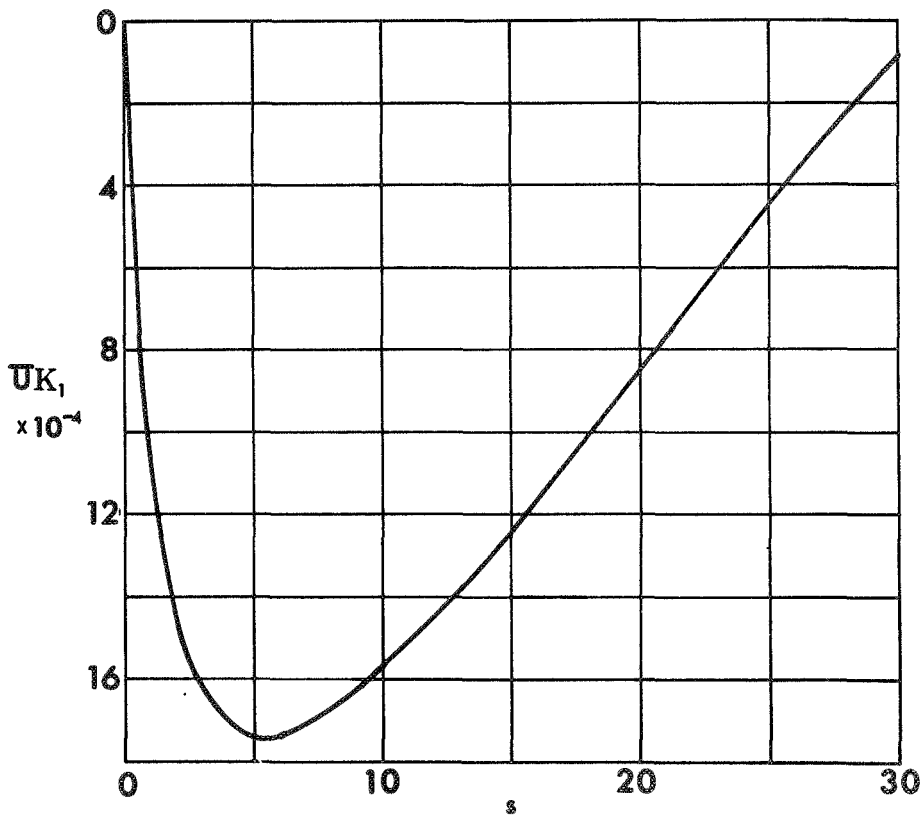

Figure C11. Inversion integrand versus independent variable, radial displacement, r/a=1.1.

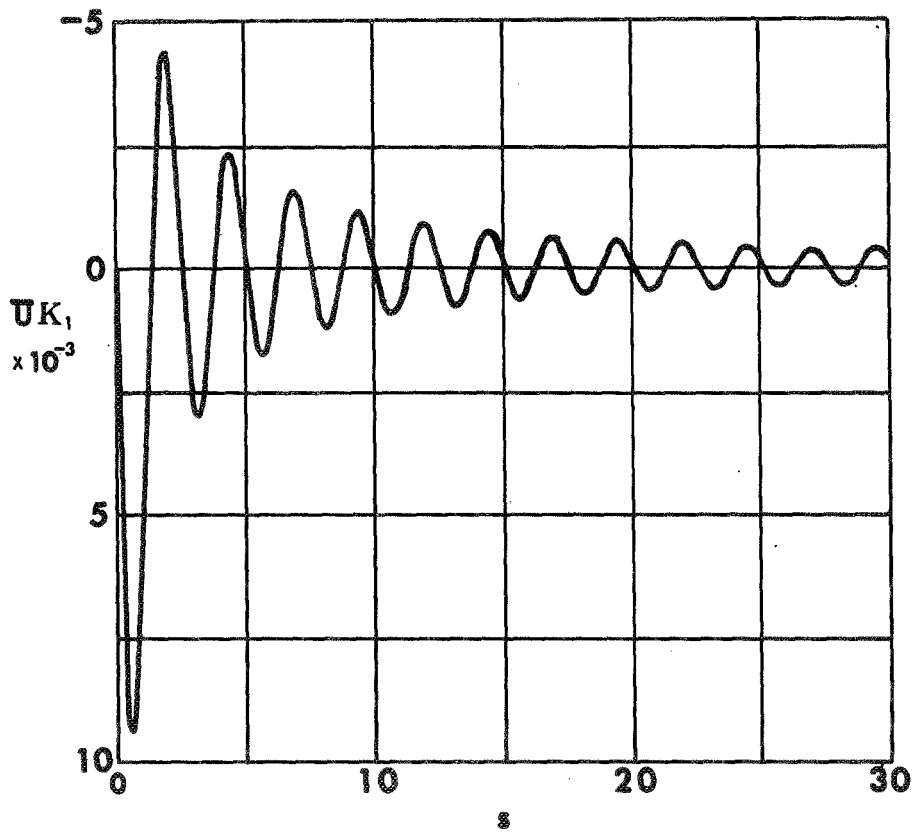

Figure C12. Inversion integrand versus independent variable, radial displacement, r/a=3.5.

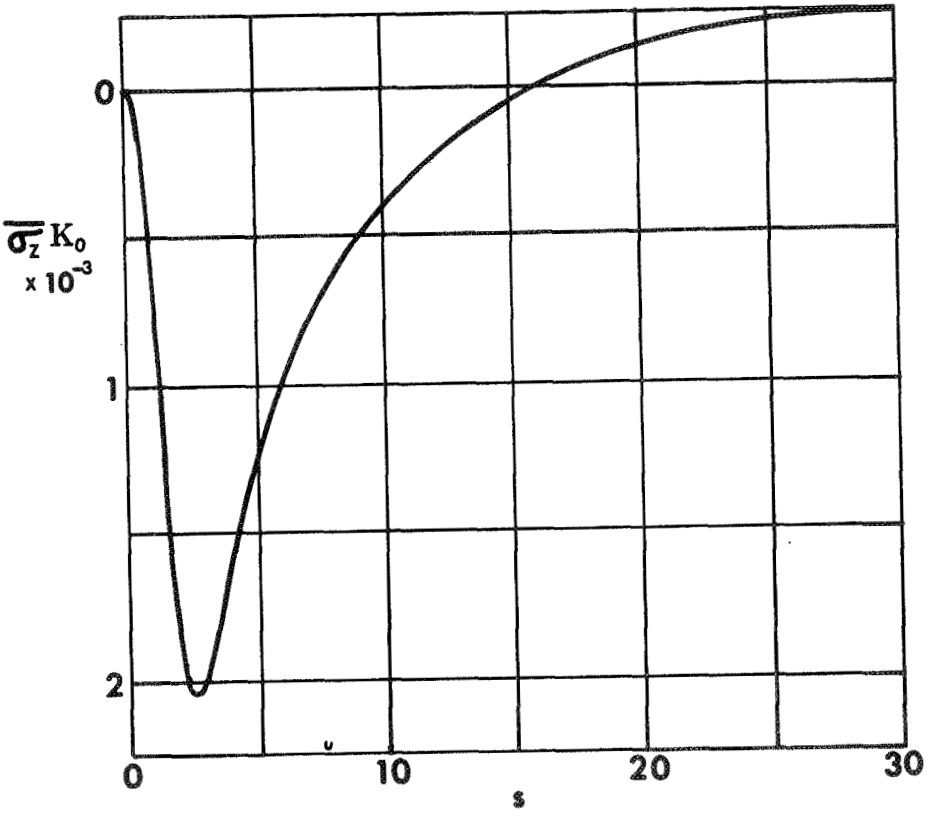

Figure C13. Inversion integrand versus independent variable, longitudinal displacement, r/a=1.1.

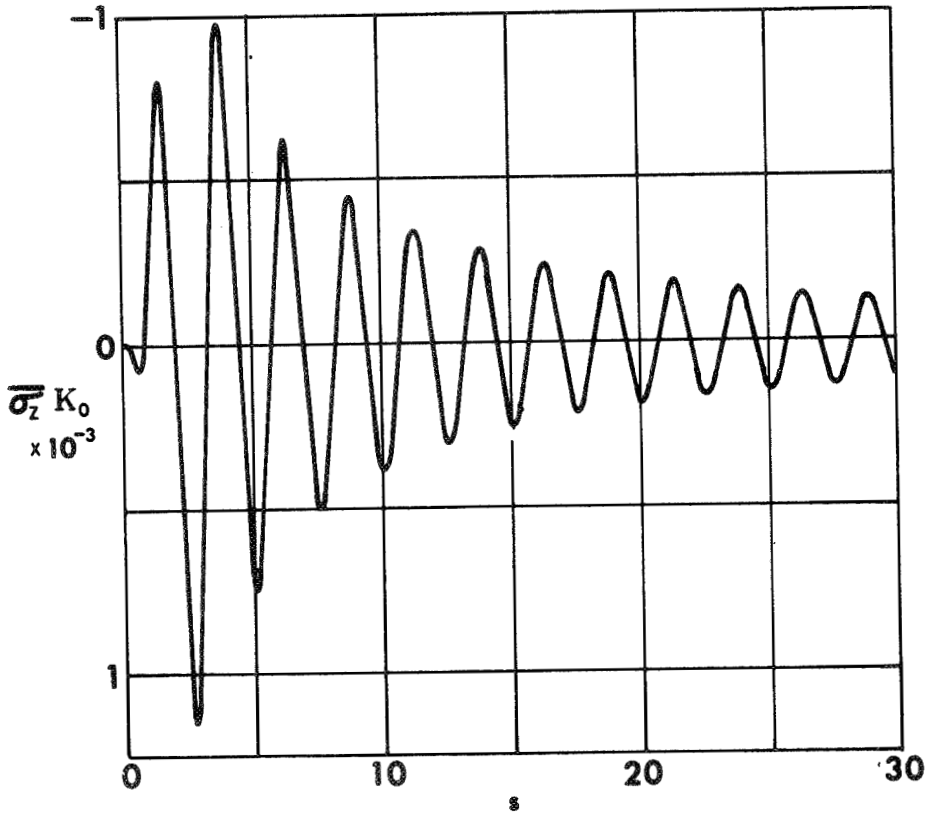

Figure C14. Inversion integrand versus independent variable, longitudinal displacement, r/a=3.5.